

# The influence of the bow shape of inland ships on the resistance

A.C. Habben Jansen

Master of Science Thesis



# **The influence of the bow shape of inland ships on the resistance**

MASTER OF SCIENCE THESIS

For the degree of Master of Science in Marine Technology at Delft  
University of Technology

A.C. Habben Jansen

June 9, 2016

Faculty of Mechanical, Maritime and Materials Engineering (3mE) · Delft University of  
Technology



Copyright © A.C. Habben Jansen  
All rights reserved.

---

# Preface

This graduation thesis is the result of a nine month during graduation project for the MSc Marine Technology programme at the Delft University of Technology. As always in science, things never finish, but my graduation project has come to an end now. Though it was an individual project and my name is on the cover of this thesis, I have received a lot of support from others, without whom this thesis would not even exist.

I would like to thank my graduation committee for their support and supervision. Though you have all given essential contributions to this project, I would like to mention my daily supervisor Erik Rotteveel first. Thanks for all good advices, support with the programming work and helping me out when I got stuck. Many thanks also go to Tom van Terwisga, my supervising professor. Thank you for the general supervision of this project and your constructive critical attitude towards my work. The third committee member from the TU Delft was Robert Hekkenberg. Many thanks go to you as well. In the beginning it was you who came up with the idea for this thesis. If I only had known then what I would sign up for... Many thanks also go to the non-TU Delft committee members. I am indebted a lot of thanks to Hoyte Raven from MARIN for the extensive support with RAPID. The results of the RAPID calculations did not only provide answers, but also many more questions, which I could discuss with you despite your filled schedule. The fifth member of my graduation committee was Jorinus Kalis from Damen Shipyards. Thank you for sharing your knowledge about the underlying physics of the resistance of inland ships. At a critical moment when I tended to get really stuck with my project, in no-time a meeting was organised at Damen to discuss the problem, which was very helpful.

Graduating is not only about knowledge, but also about persistence and motivation. In that context I would like to express my most sincere thanks to my friends. You have all experienced what graduating is like and I could share successes and sorrows with you. We started more than a year ago with counting till seven and after the defence of this thesis we will hopefully arrive at six: we (almost) made it! My final words of thanks go to my family: you have always supported me and you were interested in what I was doing, not only these past nine months, but also during the rest of my education. Thank you for your continuous support.

Agnieta Habben Jansen  
Delft, June 9, 2016



---

# Summary

Due to financial and environmental considerations there is a need to reduce the fuel consumption in the inland shipping sector. This can be realised by improving the hull design. This research focusses on the bow shape of inland ships. The bow shape with the lowest resistance is not by definition the best bow shape, since other factors such as load capacity play a role as well. Therefore it is researched what the influence of the bow shape is on the resistance. The designer could use this knowledge for finding an adequate trade-off between the resistance and the load capacity. The main research question is:

*What is the influence of bow shape parameters on the resistance of an inland ship?*

The research is limited to the ship type *Groot Rijnschip*, bulbous bows are not included and a reference stern shape is selected that remains unchanged during the research. First it has been investigated which parameters describe the bow. Eight parameters are defined: the bow length, the ship volume, the waterline entrance angle, the rake, the waterplane coefficient, the slope of the sectional area curve at two points in the bow and the ratio between to waterplane areas in the bow. A set of 133 ships with different bow shapes is generated, in which these parameters are varied in a random way. Subsequently it has been determined which parameters are relevant for sailing in restricted water. The sailing speed and water depth are selected for this.

The wave making resistance is expected to be the resistance component that is influenced most by the bow shape. Therefore the wave making resistance is calculated with the potential code RAPID for all 133 bows at eight combinations of Froude numbers and water depths. The values for the wave making resistance that are returned by RAPID are suitable for comparing the different bow shapes, but not for predicting the absolute value of the resistance. Since the calculations are carried out at low Froude numbers, the results are subjected to relative large numerical uncertainties.

Linear regression models are fitted to the results to evaluate which bow shape parameters have the largest influence on the wave making resistance. These parameters turn out to be the bow length, the ship volume and the two points that describe the slope of the sectional area curve. The way in which the parameters influence the wave making resistance is described in the models, which answers the main research questions. However, there are several

restrictions to the models: they are not able to predict the absolute value of the wave making resistance and the coefficients in the models are strongly influenced by outliers in the data obtained from RAPID. The original assumption that the viscous resistance does not change significantly has been checked with several viscous double body calculations in PARNASSOS. The results support the assumption. For practical applications, the ratio between the wave making resistance and the ship volume should be as low as possible. This results in bows shapes with a steep increase of volume at the front part of the bow and a smooth transition between the bow and the parallel midship.

For further research it is recommended to obtain a better estimate of the absolute value of the resistance. In this way it can be quantified what the influence of the bow shape on the wave making resistance means for the total ship resistance. If this more reliable data is obtained, it can be combined with data from the stern shape. In this way a detailed, adequate resistance prediction method for inland ships can be generated.

---

# Samenvatting

Vanwege financiële en economische redenen is er in de binnenvaartsector een noodzaak om het brandstofverbruik te verminderen. Dit kan worden gerealiseerd door het rompontwerp te verbeteren. Dit onderzoek focust zich op de boegvorm van binnenvaartschepen. De boegvorm met de laagste weerstand is niet per definitie de beste boegvorm, omdat andere factoren zoals het laadvermogen ook een rol spelen. Daarom is onderzocht wat de invloed van de boegvorm op de weerstand is. De ontwerper kan deze kennis gebruiken bij het vinden van een geschikte balans tussen de weerstand en het laadvermogen. De hoofdonderzoeksvraag is:

*Wat is de invloed van boegvormparameters op de weerstand van een binnenvaartschip?*

Het onderzoek beperkt zich tot het scheepstype *Groot Rijnschip*, bulbstevens worden niet beschouwd en een referentiegeometrie voor het achterschip is geselecteerd, dat niet verandert tijdens het onderzoek. Eerst is onderzocht welke parameters de boegvorm beschrijven. Acht parameters zijn gedefinieerd: de boeglengte, het volume van het schip, de invalshoek van de waterlijn, de hoek van de binnenste verticaal, de helling van de kromme van spantoppervlakken op twee punten in de boeg en de verhouding tussen twee waterlijnoppervlakken in de boeg. Een set van 133 schepen met verschillende boegvormen is gegenereerd, waarbinnen deze parameters op een willekeurige manier zijn gevarieerd. Vervolgens is bepaald welke parameters relevant zijn voor het varen in beperkt water. De vaarsnelheid en waterdiepte zijn hiervoor geselecteerd.

Er wordt verwacht dat de golfmakende weerstand de weerstandscomponent is die het meest wordt beïnvloed door de boegvorm. Daarom is de golfmakende weerstand berekend met de potentiaalcode RAPID voor alle 133 boegen op acht combinaties van Froudegetallen en waterdieptes. De waarden die RAPID geeft, zijn geschikt om de boegen met elkaar te vergelijken, maar niet geschikt om de absolute waarde van de weerstand te voorspellen. Omdat de berekeningen zijn uitgevoerd voor lage Froudegetallen, zijn de resultaten onderhevig aan relatief grote numerieke onzekerheden.

Lineaire regressiemodellen zijn gefit op de resultaten om te evalueren welke boegvormparameters de grootste invloed hebben op de golfmakende weerstand. Deze parameters blijken de boeglengte, het volume van het schip en de twee punten die de helling van de kromme

van spantoppervlakken beschrijven te zijn. De manier waarop deze parameters de golfmakende weerstand beïnvloeden is beschreven in de modellen, waarmee de hoofdonderzoeksvraag beantwoord is. Er zitten echter enkele beperkingen aan de modellen: ze zijn niet in staat om de absolute waarde van de golfmakende weerstand te voorspellen en de coëfficiënten in de modellen worden sterk beïnvloed door uitschieters in de data die verkregen is met RAPID. De oorspronkelijke aanname dat de visceuze weerstand niet significant verandert is gecontroleerd met enkele visceuze *doube body* berekeningen in PARNASSOS. De resultaten ondersteunen de aanname. Voor praktische toepassingen moet de verhouding tussen de golfmakende weerstand en het volume van het schip zo laag mogelijk zijn. Dit resulteert in boegvormen met een sterke volumetoename aan de voorkant van de boeg en een geleidelijke overgang tussen de boeg en het evenwijdige middenschip.

Voor verder onderzoek wordt aanbevolen om een betere schatting te verkrijgen van de absolute waarde van de weerstand. Op deze manier kan gekwantificeerd worden wat de invloed van de boegvorm op de golfmakende weerstand betekent voor de totale scheepsweerstand. Als deze meer betrouwbare gegevens verkregen zijn, kunnen deze gecombineerd worden met gegevens van het achterschip. Op deze manier kan een gedetailleerde, geschikte weerstandspredictiemethode voor binnenvaartschepen worden gemaakt.

---

# Table of Contents

<b>Preface</b>	<b>i</b>
<b>Summary</b>	<b>iii</b>
<b>Samenvatting</b>	<b>v</b>
<b>1 Introduction</b>	<b>1</b>
<b>2 Problem description</b>	<b>3</b>
2-1 Research objective . . . . .	3
2-2 Research questions . . . . .	4
2-3 Scope of the research . . . . .	5
<b>3 Literature overview</b>	<b>7</b>
3-1 Bow shape of inland ships . . . . .	7
3-2 Bow shape of ships in general . . . . .	9
3-3 Numerical methods for ship resistance prediction . . . . .	10
3-4 Restricted water effects . . . . .	11
<b>4 Numerical experiments</b>	<b>13</b>
4-1 Parameter selection . . . . .	13
4-2 Bow geometry generation . . . . .	16
4-3 Potential flow calculations . . . . .	20
4-3-1 Software . . . . .	21
4-3-2 Grid generation . . . . .	22
4-4 Viscous flow calculations . . . . .	24

<b>5 Results</b>	<b>27</b>
5-1 Potential flow calculations . . . . .	27
5-1-1 Wave making resistance . . . . .	27
5-1-2 Linear model generation . . . . .	31
5-1-3 Practical applications of the linear models . . . . .	39
5-2 Viscous flow calculations . . . . .	42
<b>6 Discussion</b>	<b>45</b>
6-1 Bow geometry generation . . . . .	45
6-2 Wave making resistance . . . . .	46
6-3 Linear models . . . . .	47
<b>7 Conclusions</b>	<b>51</b>
<b>8 Recommendations</b>	<b>53</b>
<b>Bibliography</b>	<b>55</b>
<b>A Alternative wave making resistance prediction method</b>	<b>57</b>
<b>B Statistical analysis plots</b>	<b>61</b>
B-1 $F_n = 0.12$ and $h = 4.0$ m . . . . .	61
B-2 $F_n = 0.12$ and $h = 5.5$ m . . . . .	62
B-3 $F_n = 0.14$ and $h = 4.0$ m . . . . .	64
B-4 $F_n = 0.14$ and $h = 5.5$ m . . . . .	65
B-5 $F_n = 0.14$ and $h = 7.0$ m . . . . .	67
B-6 $F_n = 0.16$ and $h = 5.5$ m . . . . .	69
B-7 $F_n = 0.16$ and $h = 7.0$ m . . . . .	71

---

# Chapter 1

---

## Introduction

Inland shipping plays an important role within the cargo transport sector in the Netherlands. About 35% of the Dutch inland cargo transport is covered by inland shipping. This is the largest market share that inland shipping has in Europe. The total Dutch inland shipping tonnage in 2010 was 304 million tonnes (Bureau Voorlichting Binnenvaart, 2013). The important position of the Dutch inland shipping sector is related to the presence of the Port of Rotterdam and the favourable geographical locations of the Dutch inland waterways.

The inland shipping sector currently faces some operational challenges. Firstly, there is an overcapacity of ships due to the economic crisis of 2008. In total, there are about 7000 inland ships registered under the Dutch flag (Bureau Voorlichting Binnenvaart, 2013). This results in low freight rates. To maintain a healthy financial position, there is a need for inland ship owners to save on their costs. Another point of attention in inland shipping is the environment. European emission legislation is set up to reduce the amount emission of inland ships (European Environment Agency, 2013). This obliges the inland shipping sector to search for measures that can lower the environmental impact of inland shipping.

Both the financial issue and the environmental issue are related to fuel consumption. With a decrease in fuel consumption, the costs are lowered and the environmental impact is limited. The main factors that determine the fuel consumption are the engine power and efficiency, the hull and propeller design and the navigational behaviour of the captain. This research focusses on the hull design. Details on emissions and fuel consumption of marine diesel engines can be found in Klein Woud and Stapersma (Klein Woud and Stapersma, 2012). As for the hull design, Rotteveel, Hekkenberg and Liu have evaluated the current availability of design guidelines and empirical evaluation tools for the design of inland ships (Rotteveel et al., 2014). They concluded that the design of the stern of an inland ship is more complicated than the bow design and initiated the Top Ships project for further research on this topic. This leaves further research on the bow of the ship unconsidered. However, some literature elaborates on the influence of the bow shape on the resistance. Several guidelines are mentioned by Heuser (Heuser, 1986). These guidelines are rather coarse and do not contain a sufficient level of

detail. The guidelines are composed in a time when numerical methods were not widely developed and available yet. Now that such methods are available, it is easier to investigate the influence of the bow shape on the resistance more extensively, which could probably result in more insight than the existing guidelines.

With the current need to reduce the ship resistance in the light of fuel savings and the wide availability of numerical methods, a renewed motivation for further investigation of the influence of the bow shape on the inland ship resistance arises. This is covered in this research. First, the goals and research questions are defined in Chapter 2. An overview of relevant literature is given in Chapter 3. Subsequently, numerical experiments are carried out to investigate the influence of the bow shape of an inland ship on the resistance. This is described in Chapter 4. The results of these experiments are described in Chapter 5. A discussion to place the results in the proper context is included in Chapter 6. In Chapter 7 conclusions are drawn. Chapter 8 gives several recommendations for further research.

---

## Chapter 2

---

# Problem description

In this chapter, the problem description for this research is set up. The research objective is defined in Section 2-1. In Section 2-2 the research questions are defined. Section 2-3 elaborates on the scope and limitations of the research.

### 2-1 Research objective

The objective of researching the influence of the bow shape on the resistance is to generate a method or guideline that can be used to minimise the resistance. However, the optimal bow shape is not by definition equal to the bow shape with the lowest resistance, due to economical or environmental considerations. For instance, the high cargo capacity of a rather voluminous bow can outweigh the increase in resistance of that bow. Therefore it makes sense to focus on the influence of the bow shape on the resistance rather than on the resistance itself, so that the designer can make the trade-off. This can be obtained by describing the bow with several geometrical bow shape parameters. When resistance calculations for different bow shapes are carried out, the influence of the bow shape parameters on the resistance can be determined. Statistical analysis can be used to identify which bow shape parameters have the largest influence on the resistance. In this way it can be determined which consequences choosing a certain bow shape have with regard to the resistance. This method could be used in preliminary ship design to get an idea about which bow shape is desired. More detailed CFD calculations could follow in later stages of the design. Based on this, the objective of this research can be defined as follows:

*Determine the influence of bow shape parameters on the resistance of an inland ship.*

The following definitions apply to this objective:

1. **Bow.** The part of the ship in front of the parallel midship, i.e. the front part of the ship from where the sectional area starts to reduce.

2. Bow shape parameters. Several to be chosen geometrical parameters that describe the shape of the bow.
3. Resistance. The longitudinal force that the water exerts on the ship, pointed in aft direction. The resistance can be decomposed in different components.
4. Inland ship. Representative to be chosen ship for the cargo transport fleet that sails on European inland waterways, i.e. rivers, channels and lakes.

In short, it can be stated that with this objective, it is aimed to gain more insight in the effect of the different bow shape parameters on the resistance rather than defining an optimal bow shape.

## 2-2 Research questions

The main research question can be derived directly from the objective of the research. Therefore, based on the objective defined in Section 2-1, the main research question is defined as follows:

*What is the influence of bow shape parameters on the resistance of an inland ship?*

To answer this main question, several sub-questions are defined. First, it must be determined how the bow shape can be described. The first sub-question is therefore:

1. *Which parameters describe the shape of the bow?*

Also, it should be taken into account that inland ships sail in restricted water (i.e. water of limited depth and width), which influences the resistance. This leads to the second sub-question:

2. *Which parameters are relevant for sailing in restricted water?*

When the parameters describing the bow and restricted water are defined, the resistance can be calculated for different bow shapes and waterway characteristics. The wave making resistance is expected to be the most relevant resistance component related to the bow shape (see Section 4-3). The third sub-question is therefore:

3. *What is the wave making resistance of a set of different bow shapes when the relevant parameters are varied?*

When the effect of the wave making resistance is determined, the influence of the different parameters on the resistance can be quantified with statistical analysis. In this way conclusions on the influence of the parameters on the resistance can be drawn. Therefore, the fourth sub-question is:

4. *What is the effect of the relevant parameters on the wave making resistance of the bow?*

Though the wave making resistance is expected to be the most relevant resistance component, it is acknowledged that the viscous resistance may change as well when the bow shape is changed. It is important to investigate how large this effect is. This leads to the fifth sub-question:

5. *To which extent does the viscous resistance change when the relevant parameters are varied?*

When all these sub-questions are answered, the main research question can be answered. The last step consists of presenting the results in a format that can be used in a practical way. A linear regression model is used for this.

## 2-3 Scope of the research

The Dutch inland fleet consists of various ship sizes and types. If all these types of ships would be taken into account, the amount of experiments needed to investigate the influence of the bow shape on the resistance would quickly become excessively large. Therefore, only one ship type and size is taken into account for this research. This ship type should be representative for the Dutch inland fleet. This ensures that the relevance of this research is as high as possible. For this reason, the ship type that is selected for this research is the *Groot Rijnschip*, which has the dimensions  $L = 110$  m,  $B = 11.4$  m,  $T = 3.0$  m and  $DWT = 2750$  t. The share of this ship type in the total European fleet is the largest, 38% for the dry bulk fleet and 46% for the tank fleet (Bureau Voorlichting Binnenvaart, 2013).

The second limitation of this research concerns the use of a bulbous bow. Previous research has shown that bulbous bows can result in a lower resistance, but this effect is quickly reduced when the ship sails at different limited water depths (Rotteveel et al., 2014). In practice, inland ships are commonly not equipped with a bulbous bow. For that reason, bulbous bows are not included in this research.

Since this research focuses on the bow shape, no changes are made to the stern shape. A reference stern shape is defined, which remains constant throughout the entire research. Therefore, this research does not provide any information on the influence of the stern shape on the resistance. It should be noted that interactions between the transversal bow wave system and the stern wave system may occur. This should be considered in the design of an inland ship, but this research does not cover this.

The last limitation is related to resistance prediction methods in restricted water. Both empirical and numerical methods are available. An advantage of empirical methods is that they are easy to apply. However, they are not detailed enough to take bow shape into account and they lead in general to different results (Raven, 2012). Therefore, empirical resistance prediction methods for restricted water are left outside the scope of this research. Restricted water effects are included in the numerical methods.



---

## Chapter 3

---

# Literature overview

In this chapter a literature overview is given of topics that are relevant for this research. Section 3-1 focusses on the bow design of inland ships. In Section 3-2 more general theory of bow shape design is discussed. Section 3-3 elaborates on numerical methods that are available for ship resistance prediction. In Section 3-4 aspects related to restricted water are discussed.

### 3-1 Bow shape of inland ships

The amount of publications dedicated especially to the bow shape of inland ships is limited. As mentioned in Chapter 1, Heuser gives several guidelines for the design of bow shapes for inland ships (Heuser, 1986). Within these guidelines, a distinction is made between a pontoon bow and a U-shaped bow. An example of the frame plan for both bow types is given in Figure 3-1. For a pontoon bow, the guidelines are as defined in Equations 3-1 and 3-2.

$$Lwl_{bow} \geq 5.0 \cdot T \quad (3-1)$$

$$Cb_{bow} \leq 0.75 \quad (3-2)$$

For a U-shaped bow, similar equations are defined. These are given in Equations 3-3 and 3-4.

$$Lwl_{bow} \geq 1.55 \cdot B \quad (3-3)$$

$$Cb_{bow} \leq 0.78 \quad (3-4)$$

Two parameters defining the shape of the bow are introduced. These are  $Lwl_{bow}$  and  $Cb_{bow}$ , which represent the waterline length of the bow and the block coefficient of the bow respectively. The bow is defined as the part of the ship in front of the longitudinal position where the cross-sectional area starts to reduce. It should be noted that the recommended value for  $Lwl_{bow}$  is dependent on the draught for a pontoon bow and dependent on the beam for a U-shaped bow. This is related to the water flow around the bow. For a pontoon bow, the

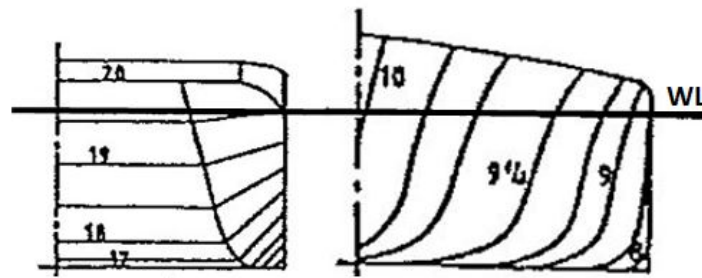


**Figure 3-1:** Example of a frame plan for a pontoon bow (left) and a U-shaped bow (right)

flow is directed mainly towards the bottom of the ship, which makes the draught a critical parameter. For a U-shaped bow, the flow is directed to the sides of the ship, so that the beam of the ship is a critical parameter. Furthermore, Heuser mentions the increasing application of the V-shaped bow. The design guidelines for this bow are equal to those for the conventional bow. The V-shaped bow combines a high load capacity with good flow characteristics.

In another publication, Heuser describes the historical development of bow shapes of German inland ships (Heuser, 1987). Since the 60's of the last century, pontoon bows were increasingly applied due to the low building costs. The fact that this bow shape results in a rather high resistance and thus high fuel costs, was deemed less important due to the low oil price. Due to the fast increase in oil prices in the oil crises of 1974 and 1978, the interest in designing a ship with better resistance characteristics was renewed. This had led to the application of the V-frame shaped bow for ships in extreme shallow water and seagoing inland ships. For navigation on rivers and channels, a bow with parabolic waterlines was regarded most suitable.

Van Terwisga gives a literature overview (van Terwisga, 1989) of the resistance and propulsion of barges. The bow shape is explicitly mentioned in this overview. Graphs are presented for the influence of several angles and radii of the bow on the total resistance coefficient, sinkage and trim. These graphs are based on empirical experiments. It turns out that the resistance coefficient decreases when the rake, i.e. the angle of the beveled bottom, is increased. Furthermore, the influence of the waterline entrance angle in the horizontal waterplane is investigated. A value of 20 degrees leads to the smallest resistance coefficient. However, these experiments apply to barges with straight buttocks and waterlines. These barges are usually pushed, towed or coupled and do not necessarily represent current bow shapes of inland ships.

In a literature overview of Rotteveel, Hekkenberg and Liu it is stated that the effects of applying a bulbous bow have been investigated (Rotteveel et al., 2014). It turns out that the beneficial effect of the bow diminishes when the water depth is limited. Furthermore, a bulbous bow has a beneficial effect for the design draught only. Since inland ships are exposed to large differences in water depth and draught, it is expected that the benefits of a bulbous bow are not significant.

## 3-2 Bow shape of ships in general

Though the amount of publications dedicated to the bow design of inland ships is limited, several guidelines for bow design in general can be found. Though this does not directly apply to inland ships, it could be useful to evaluate these guidelines to gain more insight in which parameters are relevant.

As for the design of the bow, Watson starts with mentioning that it has to be decided whether or not a bulbous bow should be applied (Watson, 1998). He presents a table that indicates the advantage of a bow based on a combination of the block coefficient and the Froude number. Inland ships usually have a high block coefficient and a (very) low Froude number. According to this table, a conventional bow, i.e. a bow without a bulb, is superior for this combination. The table does not include water depth, but since a limited water depth decreases the usefulness of a bulbous bow only further, it can be concluded that a conventional bow is indeed superior for inland ships. Furthermore, Watson advises to apply forward rake and bow flare to reduce pitching, water on the fore deck and damage in case of collision. Pitching and water on the fore deck do usually not apply to inland ships, but adapting the bow shape such that collision damage is reduced is a factor that can be taken into account. It is also mentioned that the bow flare should not be exaggerated, since this can cause high torsional vibrations due to waves. However, extreme wave conditions do not appear at inland waters.

Schneekluth and Bertram elaborate further on conventional bows. They mention the same advantages of forward rake as Watson, but point out that a reduced rake is frequently applied when the overall length of the ship is restricted (Schneekluth and Bertram, 1998), which is the case for inland ships. Furthermore, they compare U- and V-shaped bows. It turns out that a V-shaped bow has numerous advantages, such as a higher stability value  $KM$  and a larger deck area. It also turns out that V-shaped bows have a higher wave making resistance and a lower frictional resistance than U-shaped bows. For low Froude numbers, i.e.  $Fn < 0.18$ , which is the case for inland ships, this means that the total resistance is smaller when a V-shaped bow is applied. This also applies for high Froude numbers and ships with a high  $B/T$  ratio. Schneekluth and Bertram also consider the shape of the forward waterlines. Based on the prismatic coefficient of the hull, a value for the waterline half-angle of entry is recommended based on the method of Pophanken. This angle is also dependent on the  $L/B$  ratio. Furthermore, it is mentioned that a parabolic bow is often applied to ships with  $Cb > 0.8$  and  $Fn < 0.18$ , which applies to inland ships. A parabolic bow has elliptical waterlines. The minor axis of the ellipse equals the beam of the ship.

Larsson and Raven also mention the importance of reducing the waterline entrance angle and add that the slope of the sectional area curve at the bow should be kept to a minimum (Larsson and Raven, 2010). When the waterline entrance angle is small and the slope of the sectional area curve is high, hollow waterlines occur, which is an undesirable situation. In practice, these two requirements conflict, which means that a trade-off should be made. It is mentioned that nearly straight waterlines are a good compromise, but this is probably the result of increased knowledge on bulbous bows. Therefore, this does not necessarily apply to inland ships.

### 3-3 Numerical methods for ship resistance prediction

Various numerical methods are available to calculate the resistance of ships. These methods range from basic and robust to extensive and very accurate. The following types of numerical resistance prediction methods are used commonly:

1. Panel methods (e.g. RAPID, DelKelv). These methods are able to calculate the wave making resistance and the wave pattern of a ship. Its basis is the Laplace potential equation (de Koning Gans, 2012). Since this equation does not handle viscosity, the panel method does not include frictional resistance. The Laplace equation has three dimensions and considers the control volume in which the ship hull is modelled. By using Green's identity, the three-dimensional Laplace equation can be reduced to a two-dimensional surface integral. The surface consists of the hull of the ship and the free water surface. To solve the integral, the surface is subdivided in small panels (grid generation). An unknown source strength is associated with each panel. All sources together create the flow around the hull. Making use of the boundary conditions, the unknown source strengths can be solved. Subsequently, velocities and pressures in the grid can be calculated. Advantages of panel methods are that they are fast and that only a surface grid instead of a three-dimensional grid has to be made. Calculations are in general finished within several minutes. A disadvantage is that panel methods are not able to compute the stern wave profile accurately due to the neglect of viscosity.
2. CFD methods with structured grid (e.g. PARNASSOS). These methods calculate the viscous flow around a ship hull. This means that all resistance components are taken into account, contrary to panel methods. PARNASSOS is an example of this method for dedicated maritime applications (MARIN, 2015a). This program is based on solving the Reynolds-averaged Navier-Stokes (RANS) equations. This means that the Navier-Stokes equations for the flow around the hull are decomposed into a steady and a fluctuating part. In this way, turbulence can be included in the computations. Dense grids are allowed, such that a high numerical accuracy is obtained. The domain is subdivided in blocks, which are filled with a structured grid. A typical calculation is in general finished within a day. The program is suited for ships without appendages or complex geometries, but does not handle wave breaking. It can be chosen to calculate both the double body flow and the flow with a free surface.
3. CFD methods with unstructured grid (e.g. ReFRESCO, FINE/Marine). The basis of these methods is similar to CFD methods with a structured grid. However, there are some differences that make it possible to handle more complex situations. ReFRESCO solves the RANS equations (MARIN, 2015c), just as PARNASSOS, but additionally allows multi-phase flows and uses the volume-fraction transport equations. These equations are used in a free-surface modelling technique that numerically locates the free surface. This method is also suited for calculating breaking waves. FINE/Marine has similar functionalities (Numecca International, 2015). Calculations with this CFD method are usually expensive and time consuming.

From this, it can be concluded that the choice for the resistance prediction method is governed by the desired accuracy of the result and the available time. Numerical ship resistance

prediction methods are also able to handle shallow water effects. This is further explained in Section 3-4.

### 3-4 Restricted water effects

The term "restricted water" refers to water of both limited depth and width. Most literature elaborates on the limited depth. When only limited depth is considered, the term changes to "shallow water". When a ship sails in shallow water, the resistance increases compared to when the ships sails in deep water. This is caused by three major shallow water effects, of which an overview is given by Raven (Raven, 2012):

1. Viscous flow and form factor. Due to the presence of the waterway bottom, the flow direction is more horizontal than for deep water. This results in larger pressure gradients, resulting in an increasing form factor. This effect is governed by geometric parameters such as  $h/T$  or  $Am/h^2$ .
2. Wave making and wave resistance. For moderate to high sailing speeds, the waves produced by the ship are relatively long. The pressure distribution farther beneath the water surface influences this effect. Due to the presence of the waterway bottom, the wave amplitude and resistance increase for moderate speeds. For high speeds, the wave length and shape is effected by the waterway bottom. This is associated with a significant increase of the wave resistance. The governing parameter for this effect is the Froude depth number (Equation 3-5). The speed where  $Fn_h = 1$  is known as the critical speed. Towards this speed, the wave resistance increases maximal.

$$Fn_h = \frac{V}{\sqrt{gh}} \quad (3-5)$$

3. Sinkage and trim. Due to the lower pressure between the bottom of the ship and the bottom of the waterway, a sailing inland ship is exposed to sinkage. Furthermore, the trim is changed. The extra draught increases both the wave resistance and the viscous resistance. The governing parameters of this effect are the same geometric parameters as mentioned in effect 1.

It is also mentioned that shallow water has effect on the hull efficiency and the open water efficiency. However, these effects are not clear yet. These two shallow water effects are not related to the bow of the ship.

When the width of the waterway is also limited, additional effects may occur, due to blockage. A measure for the blockage is the blockage factor  $\beta$  (Equation 3-6), which is the ratio between the midship sectional area and the cross-sectional area of the waterway. In this equation,  $w$  denotes the width of the waterway.

$$\beta = \frac{Am}{w \cdot h} \quad (3-6)$$

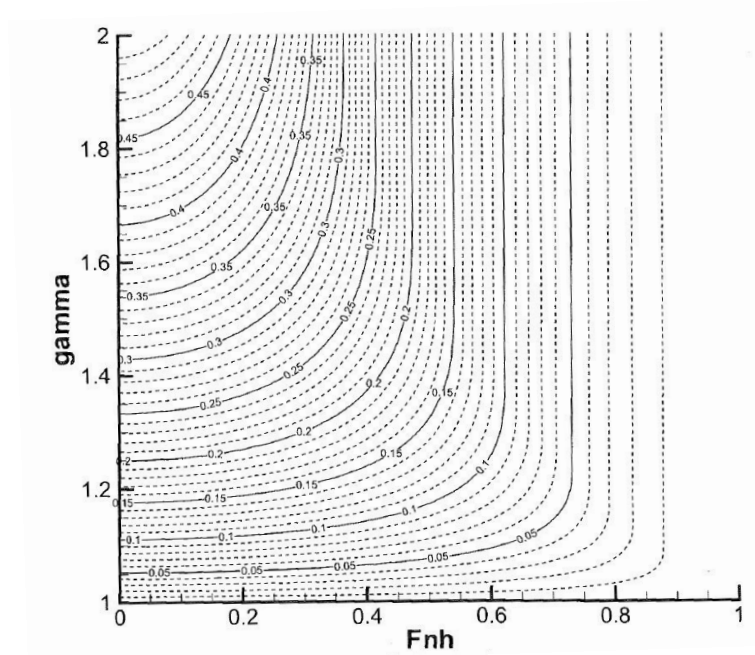


**Figure 3-2:** Kreitner's diagram

When this blockage is significant, the overspeed next to the hull increases, resulting in increased sinkage, pressure gradients, wave amplitudes and viscous resistance. Larsson and Raven discuss Kreitner's theory (Larsson and Raven, 2010), which is a method to assess these effects. The basis of Kreitner's theory is the overspeed ratio  $\gamma$ , which is the ratio between the increased ship speed next to the hull and the sailing speed. The relation between the blockage, the overspeed ratio and the Froude depth number is given in Equation 3-7.

$$\gamma \left( 1 - \beta - \frac{1}{2} Fn_h^2 [\gamma^2 - 1] \right) = 1 \quad (3-7)$$

From this equation, the overspeed ratio can be determined for a given blockage and Froude depth number. It turns out that for a certain Froude depth number, the overspeed ratio increases very fast, which is represented by the vertical asymptotes in Figure 3-2. The value of this Froude depth number is dependent on the blockage. This phenomenon is the result of the water level depression that occurs next to the ship according to Bernoulli's law. It leads to a very high increase in resistance and violent flow phenomena. The sailing speed related to this Froude depth number is known as the critical channel speed.

In most numerical methods, an option is available to include limited water depth and width. In RAPID, the grids of the hull and the surface are mirrored with respect to the bottom plane. This results in similar source strengths as in the original grid, but with an opposite direction. It ensures that no water flow through the bottom occurs. Another method is to cover the bottom with panels. CFD codes use a three-dimensional grid. Restricted water effects can be imposed by limiting the domain size and refining the grid near the waterway bottom and walls.

# Numerical experiments

In order to answer the research questions defined in Section 2-2, experiments are carried out. The goal of this experiments is to determine the resistance for a set of ships with varying bow shapes. Resistance experiments can be performed both empirically (in a towing tank) or numerically (with dedicated software). Since multiple bow shapes are to be investigated, the amount of experiments is rather large. This imposes major practical difficulties for empirical experiments. Numerical experiments, on the other hand, can be easily performed in large numbers. Therefore only numerical experiments are carried out for this research. First, it has to be determined which parameters will be varied. This is described in Section 4-1. Subsequently, the geometry for the different bow shapes has to be generated. Section 4-2 elaborates on this. Both potential flow and viscous flow calculations are carried out. This is discussed in Sections 4-3 and 4-4, respectively.

### 4-1 Parameter selection

The first two research questions can be answered with the literature research of Chapter 3. First it has been determined which parameters describe the bow. Based on the publications of Heuser, it can be concluded that the bow length and the block coefficient of the bow are important geometrical parameters that describe the bow of inland ships. However, investigating the influence of the block coefficient of the bow on the resistance is not possible, since the block coefficient of the bow is dependent on the bow length. For example, a ship with a large bow length and a large block coefficient of the bow could have less displacement than a ship with a short bow and a small bow block coefficient, even though its block coefficient is larger. Therefore it is better to use the total ship displacement as a parameter in this research.

In the publications of Watson, Schneekluth & Betram and Larsson & Raven, several other parameters that describe the bow can be found. They mention the rake and the waterline entrance angle. These parameters will also be included in this research. It is expected that the waterline entrance angle has in particular a large influence on the resistance, since this

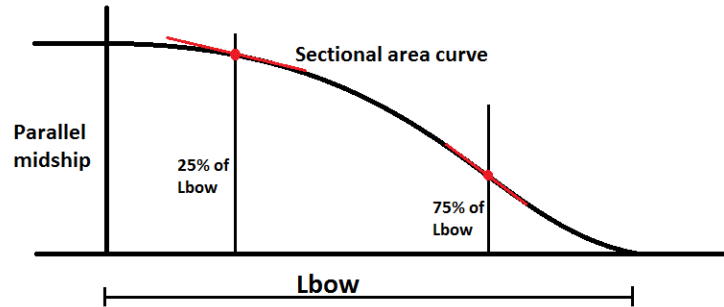


**Figure 4-1:** Graphical representation of the points describing the slope of the sectional area curve

parameter determines to which extent the water flow along the ship is redirected. However, more parameters are required to describe the shape of the waterlines. To describe whether the shape of the waterline area of the bow is full or slender, the waterplane coefficient of the bow is introduced. Furthermore, Larsson & Raven mention the importance of the slope of the sectional area curve. This slope will be evaluated at two longitudinal points. The value of the sectional area curve at 25% of the bow length can be used as a measure for the sharpness of the forward shoulder. Furthermore, the value at 75% of the bow length is introduced. In combination with the waterline entrance angle, the slope of the sectional area curve at this point is a measure for the curvature of the waterline. The bow length is measured from the end of the parallel midship. Figure 4-1 gives a graphical representation of the two points of the sectional area curve. The previous mentioned parameters are related in particular to the shape of the waterline. It can also be interesting to investigate the distribution of the bow volume over the draught. When a major part of the volume is located near the bottom, the frames are U-shaped. A concentration of the volume near the waterline indicates a more V-shaped bow. A measure to quantify this has been defined by taking the ratio of the waterplane area at 25% of the draught and the waterplane area at 100% of the draught. When this ratio is high, it indicates that a large part of the volume is located near the bottom. Similarly, the ratio of the waterplane area at 75% of the draught and the waterplane area at 100% of the draught is introduced. This ratio indicates how much volume is located near the waterline.

In total, nine parameters are set up to describe the shape of the bow. These are not the only possible parameters that describe the bow shape. For instance, other parameters could be the prismatic coefficient of the bow or the radius of the bow frames. However, caution should be taken with adding extra parameters, since they may interact with each other and the bow geometry generation becomes more complex. Therefore, no extra parameters than the previous mentioned parameters that are based on literature research are chosen. An overview of them is given in Table 4-1. For a proper analysis of the results of the experiments, it is important to ensure that the parameters are independent. Furthermore, the parameters should be varied within a proper design space. Section 4-2 elaborates further on this.

Apart from selecting parameters that describe the bow, it has been determined which parameters should be taken into account for sailing in shallow water. From the literature research of Chapter 3 it turns out that two parameters are of particular importance. These parameters are the sailing speed and the water depth. To limit the amount of experiments needed, only

**Table 4-1:** Geometrical parameters describing the bow shape

Parameter	Symbol	Unit
Bow length	$L_{bow}$	$m$
Ship volume	$\nabla$	$m^3$
Waterline entrance angle	$\alpha$	$deg$
Rake	$\beta$	$deg$
Waterplane coefficient	$C_{wp}$	–
Slope of Sectional Area Curve at 25% of bow length	$SAC_{25}$	–
Slope of Sectional Area Curve at 75% of bow length	$SAC_{75}$	–
Ratio of waterplane areas at 25% and 100% of draught	$T_{25}$	–
Ratio of waterplane areas at 75% and 100% of draught	$T_{75}$	–

**Table 4-2:** Froude depth numbers for different combinations of Froude numbers and water depths

<b>Fn   h [m]</b>	<b>4.0</b>	<b>5.5</b>	<b>7.0</b>
<b>0.12</b>	0.629	0.536	0.476
<b>0.14</b>	0.734	0.626	0.555
<b>0.16</b>	0.840	0.716	0.635

three values for these parameters are selected: a low, average and high value. In this way, it is possible to compare the different bow shapes within several combinations of water depths and sailing speeds. The maximum value for the water depth is set to 7.0 m. At this water depth, shallow water effects are expected to be limited. This makes it easier to identify the shallow water effects at lower water depths. The lowest value of the water depth is set to 4.0 m. Since the draught of the ship is 3.0 m, the under keel clearance for this situation is 1.0 m, which will in practice be needed for safe navigation. For the sailing speed, the minimum value is set to 14 km/h, which is slightly above the required minimum speed for navigation on the Rhine (Netherlands Government, 1995). The maximum value for the sailing speed is set to 19 km/h, which is the practical upper speed limit within inland shipping. Since the used software expresses the sailing speed as Froude numbers, the minimum and maximum sailing speed are expressed as  $Fn = 0.12$  and  $Fn = 0.16$ , respectively. This leads to nine possible combinations of water depths and Froude numbers, as presented in Table 4-2. The entries of the table present the Froude depth number for each situation. The combination of  $Fn = 0.16$  and  $h = 4.0$  m is not considered, since the associated Froude depth number imposes difficulties for the software. Furthermore, this is not a realistic situation for sailing in practice.

Though the width of the waterway is not taken into account in this research, it is important to keep in mind that when the waterway width is too limited, additional resistance effects may occur that are not covered with this research. As discussed in Chapter 3, a critical channel speed can be derived for a given blockage factor with the Kreitner diagram. This diagram can also be used the other way around. With a given Froude depth number, a critical blockage, thus a critical waterway width, can be determined, assuming a rectangular cross-section of the waterway. This gives an indication of the minimal width of the waterway that is required to avoid serious additional resistance due to a limited width. This minimal required waterway

**Table 4-3:** Critical waterway widths [m]

<b>Fn</b>   <b>h [m]</b>	<b>4.0</b>	<b>5.5</b>	<b>7.0</b>
<b>0.12</b>	95	41	26
<b>0.14</b>	171	69	35
<b>0.16</b>	N/A	104	54

width is given for each situation in Table 4-3. It is very important to realise that these values can only be used as an indication, since Kreitner's theory and the analysis made here are subjected to several assumptions and simplifications that may not apply to for all cases.

## 4-2 Bow geometry generation

Before performing the numerical resistance experiments, a set of bow shapes has to be generated. It has to be taken into account to which extent the bow shape parameters have to be varied. According to the theory of Design of Experiments, parameters in an experiment can be chosen in three different ways. These comprise a full factorial design, a fractional factorial design or a random design. In a full factorial design, different values for the parameters are chosen at a certain number of levels. Subsequently, experiments are carried out for each possible combination of parameters. This approach is suited for experimental set-ups with few parameters at few levels. The number of parameters of this research is too large to use this experimental design. To illustrate: this research covers nine bow shape parameters. Assume they would be set to three different levels. Then  $3^9 = 19683$  different bow shapes would be needed. Even more experiments would have to be executed, since different Froude numbers and water depths are covered. Therefore, a full factorial design for the experiments is not a practical option. An option could be to use only a fraction of the full factorial design (fractional factorial design). However, this method still requires that the values of the parameters are set at several constant levels. In practice, it is difficult to generate bow shapes in which the parameters defined in Section 4-1 have values at predefined constant levels. This is difficult because values of the bow shape parameters are a result of the lines plan rather than values where the lines plan is based on. A random design seems to be the most promising approach. This approach is suitable for investigating the effects of a larger amount of parameters with a limited number of experiments. Furthermore, it is easier to generate bow shapes with a random distribution of parameters than setting each parameter to constant levels. This means that first the bow shapes are generated in a random way. The values for the parameters are determined afterwards.

The different bow shapes are generated in Rhinoceros 5.0 (Rhino) in combination with a script in Python. The basis for the script was already available. The script has been modified such that different bow shapes are generated automatically. These bow shapes consist of six curves. Each curve is defined by three points. These points are located at the centerline, in the bilge and and at the deckline. Based on the three points, a third-degree polynomial is generated. The point at the bilge is a control point with an associated weight. The weight determines the radius of the curve. An example of a curve with its associated points is given in Figure 4-2.

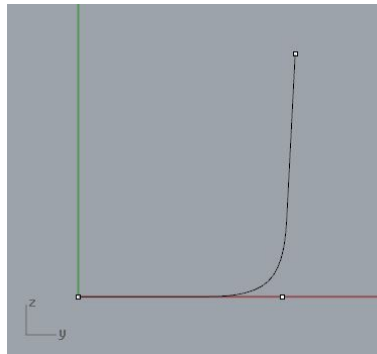


**Figure 4-2:** Example of bow curve

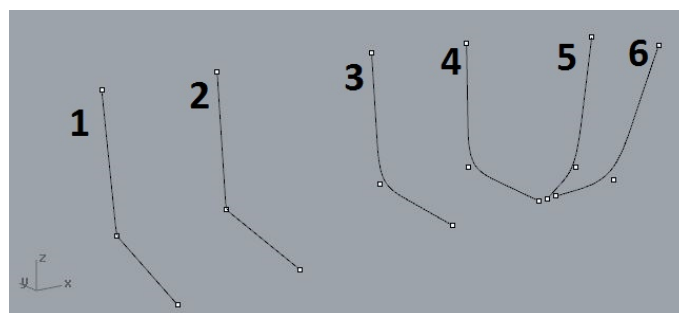


**Figure 4-3:** Overview of bow curves

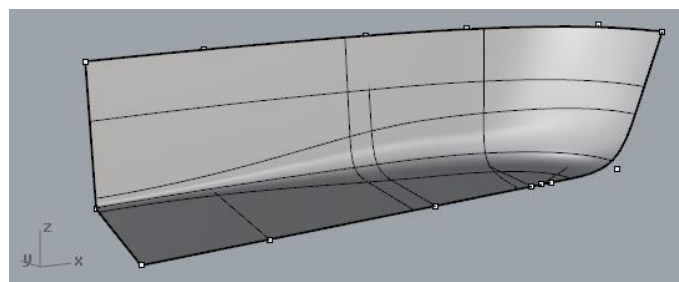


**Figure 4-4:** Example of bow shape generated with loose loft function

An overview of all bow curves together is given in Figure 4-3. Curves 1 to 4 are placed orthogonal to the centerplane of the ship. Curve 1 coincides with the forward end of the parallel midship. Curve 6 is the most forward curve and represents the contour line of the bow. This curve coincides with the centerplane of the ship. Curves 2 to 4 are placed at 20%, 50% and 70% of the bow length, respectively. The shape of curve 2 is identical to the shape of curve 1 to obtain a smooth connection between the parallel midship and the bow. Curve 5 is placed under an angle of 30 degrees with the centerplane. The radius between the bottom and the side increases over the bow length. A surface is lofted through the curves. Various loft types are available. For this research, a loose loft is applied. With this loft type, the control points of the surface are equal to the control points of the curves. A third-degree surface is generated with the curves as basis. This method is especially suitable for situations where shapes are modified, which is the case in this research. An example of a bow shape generated in this way is presented in Figure 4-4.

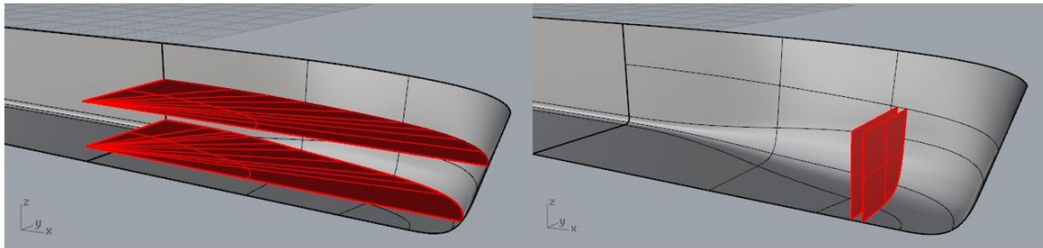


**Figure 4-5:** Definition of the surfaces from which  $T25$  and  $SAC75$  are derived

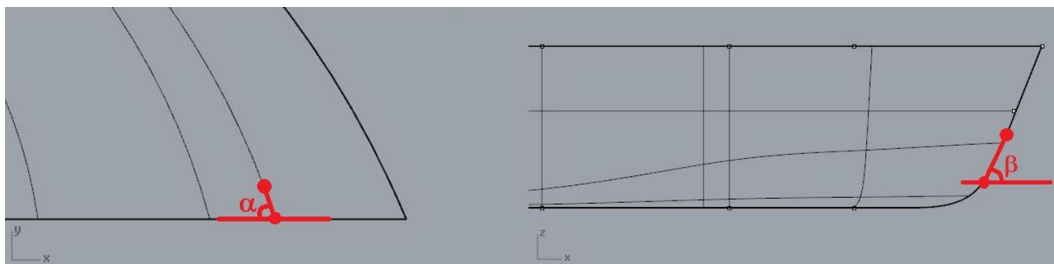


**Figure 4-6:** Definition of waterline entrance angle and rake

The variation in bow shapes is obtained by varying the longitudinal location of the aft end of the bow and shifting points on curves 3 to 6. For curves 3 and 4, the deck line and bilge points can be shifted transversely. For curve 5, the deck line and bilge points can be shifted horizontally along the direction of the curve (30 degrees with the centerplane). For curve 6, the bilge point can be shifted in longitudinal direction. The deck line point of curve 6 is fixed at 110 m, to maintain the over all ship length. The rate in which the points are shifted, is determined with Latin Hypercube Sampling. This is a statistical method for generating a random collection of parameter values for experiments. In this case, the parameter values are the locations of the points. The parameter values are distributed equally over the design space. In total, 400 combinations of parameter values are generated with MATLAB. The output consists of numbers between 0 and 1. Minimum and maximum values for the locations of the points are defined, between which the points are shifted with a distance based on these numbers. However, since the location of the points is determined randomly, the set of generated bows also contains unrealistic bow shapes. To select the realistic bow shapes only, three criteria are defined:

1. Within a curve, the bilge point is located closer to the centerline than the deck line point.
2. The transverse location of the deck line points and bilge points is continuously decreasing.
3. The longitudinal location of the deck line points and bilge points is continuously increasing.

From the 400 bow shapes that are generated, there are 133 that meet the criteria. This are enough bow shapes for continuing the research. There are nine parameters that are

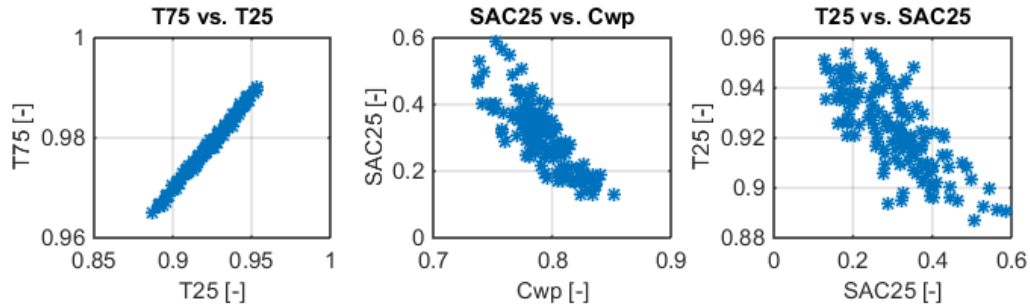
investigated. These parameters will eventually be used in a linear regression model to investigate their influence on the wave making resistance. At the moment it is not yet clear which of these parameters are to be included in the model. If it is assumed for now that a quadratic model is required, then this would result in 55 unknowns (9 linear terms, 9 quadratic terms, 36 interaction terms and an intercept term). Then at least 55 experiments would be required. This is supported by literature. For example, Wang recommends  $(n+1)(n+2)/2$  experiments, where  $n$  is the number of parameters (Wang, 2003). For nine parameters, this leads indeed to 55 experiments. In another study on the influence of the hull shape on the wave making resistance, 60 experiments are applied for 16 design variables (Kim et al., 2011). However, the more experiments are carried out, the better the data is for constructing the regression model. For these bow shapes, the geometrical parameters defined in Section 4-1 are calculated. One set of points leads to only one set of parameters and vice versa. This is because the location of a point influences multiple parameters. For instance: a point on the deck line influences the waterline entrance angle ( $\alpha$ ), the waterplane coefficient ( $C_{wp}$ ) and the slope of the sectional area curve ( $SAC_{25}$  and  $SAC_{75}$ ). A point on the bilge line influences the slope of the sectional area curve and the waterplane ratio ( $T_{25}$ ). Furthermore, all points influence the ship volume ( $\nabla$ ) and the bilge point of the most forward curve influences the rake ( $\beta$ ). Therefore, it is not possible to generate a certain combination of parameters with more than one combination of points. Most parameters are based on areas and volumes and are therefore easy to obtain from Rhino. As illustration, the surfaces from which the parameters  $T_{25}$  and  $SAC_{75}$  are derived are presented in Figure 4-5. For the parameters denoting an angle, i.e. the waterline entrance angle and rake, the following definitions apply, which are visualised in Figure 4-6:

1. Waterline entrance angle: the angle between the centerline and the inclined line between the points located most forward and at 1% of the waterline length of the bow.
2. Rake: the angle between the horizontal plane and the inclined line between the points located at 25% and 75% of the draught at the bow contour.

After the values of the parameters are obtained for the 133 bow shapes, it has been investigated whether relations exist between the parameters. For investigating the effect of the different parameters on the resistance, it must be ensured that the parameters are independent. It cannot be prevented that there will be a certain rate of dependency between several parameters, but this should be kept to a minimum. A way to quantify this is the  $R^2$  value. When this value is high for a combination of parameters, it indicates that a dependency between the two parameters exists. For every possible combination of parameters the  $R^2$  value has been calculated. The result is presented in Table 4-4. For the highest three  $R^2$  values the according data is plotted. This is presented in Figure 4-7. From the left graph of this figure it can be concluded that there is a strong relation between how much volume is located near the waterline and how much volume is located near the bottom. This is because the method for the generation of bow shapes uses points on only two different heights. More variation could be obtained by adding flare, but inland ships usually do not have flare. Therefore, taking only one of the two parameters into account is sufficient. The parameter  $T_{25}$  is selected, since the scatter of this parameter is larger. For the other two graphs in Figure 4-7 there is also a certain correlation, but this is less distinct than for the correlation between  $T_{25}$  and  $T_{75}$ . Therefore these parameters are not excluded from the evaluation. The boundary value

**Table 4-4:**  $R^2$  values for combinations of parameters

Par 1	Par 2	$R^2$	Par 1	Par 2	$R^2$	Par 1	Par 2	$R^2$
$T_{25}$	$T_{75}$	0.991	$C_{wp}$	$T_{75}$	0.240	$\alpha$	$SAC_{75}$	0.027
$C_{wp}$	$SAC_{25}$	0.669	$\nabla$	$SAC_{25}$	0.227	$\beta$	$SAC_{25}$	0.017
$SAC_{25}$	$T_{25}$	0.554	$C_{wp}$	$SAC_{75}$	0.224	$L_{bow}$	$T_{25}$	0.016
$\nabla$	$C_{wp}$	0.527	$L_{bow}$	$\alpha$	0.201	$L_{bow}$	$C_{wp}$	0.015
$SAC_{25}$	$T_{75}$	0.503	$\nabla$	$\alpha$	0.199	$\alpha$	$\beta$	0.012
$\nabla$	$SAC_{75}$	0.494	$L_{bow}$	$SAC_{75}$	0.181	$\alpha$	$T_{25}$	0.011
$\nabla$	$T_{75}$	0.310	$SAC_{25}$	$SAC_{75}$	0.179	$\alpha$	$SAC_{25}$	0.009
$\nabla$	$T_{25}$	0.287	$L_{bow}$	$SAC_{25}$	0.164	$\alpha$	$T_{75}$	0.009
$L_{bow}$	$\nabla$	0.282	$\beta$	$T_{75}$	0.084	$L_{bow}$	$T_{75}$	0.006
$SAC_{75}$	$T_{75}$	0.263	$\alpha$	$C_{wp}$	0.084	$\beta$	$C_{wp}$	0.004
$C_{wp}$	$T_{25}$	0.261	$\nabla$	$\beta$	0.063	$\beta$	$SAC_{75}$	0.001
$SAC_{75}$	$T_{25}$	0.254	$\beta$	$T_{25}$	0.062	$L_{bow}$	$\beta$	0.000

**Figure 4-7:** Relation between parameters with highest  $R^2$  values

of  $R^2$  up to which parameters are considered independent is therefore set to 0.669 (see Table 4-4). This should be taken into account during the statistical analysis of the results. Eight parameters remain for investigating the influence of the bow shape on the resistance. The range in which the parameters are varied can now be derived from the data. This is presented in Table 4-5.

### 4-3 Potential flow calculations

As stated in Section 2-2, it is expected that the wave making resistance is expected to be the most relevant resistance component with regard to the bow shape. The reason for this is that the surface of the bow has components that are perpendicular to the flow. This results in pressure build-ups, which on its turn results in the generation of a bow wave system. Furthermore, the viscous boundary layer has a limited thickness at the bow, since it is the front part of the ship. Viscous effects are expected to be more relevant in the parallel midship and the stern. Since the focus lies on the wave making resistance, potential flow calculations are carried out first. These are described in this section. Paragraph 4-3-1 elaborates on the numerical tool that is used for the experiments. In Paragraph 4-3-2 it is described how the grids are generated.

**Table 4-5:** Minimum and maximum values of the evaluated parameters

Parameter	Minimum value	Maximum value	Unit
$L_{bow}$	17.0	24.0	$m$
$\nabla$	2845	2992	$m^3$
$\alpha$	57.8	86.3	$deg$
$\beta$	65.3	75.0	$deg$
$C_{wp}$	0.737	0.852	–
$SAC_{25}$	0.129	0.587	–
$SAC_{75}$	0.529	1.452	–
$T_{25}$	0.887	0.954	–

### 4-3-1 Software

As described in Section 3-3, panel codes are suitable methods for potential calculations. For this research the panel code RAPID is used (MARIN, 2015b), which is developed at MARIN. RAPID is chosen since it practical in use and compatible with the grid generation method in Rhino. Another major advantage is that RAPID considers the full non-linear free surface conditions. RAPID calculates the wave profile and returns two values for the wave making resistance. The first value is  $Rw1$ , which is calculated by integrating the pressures over the wetted surface. The second value is  $Rw3$ , which is calculated by making a transverse cut of the wave profile behind the stern. Due to the consideration of the non-linear free surface conditions, the two calculation methods are theoretically equal. RAPID is an iterative numerical method that follows several steps until convergence is obtained (Raven, 1996). First, an initial approximation of the free surface and the velocity distribution is set up. Then a panel distribution is defined on the hull and above the free surface. Each panel is associated with a collocation point. For the free surface, the collocation points are at the same height of the free surface. All collocation points have an unknown source strength. These source strengths can be solved with appropriate boundary conditions. When the source strengths are known, the pressure and velocity fields can be calculated. This results in an updated free surface. Furthermore, the resistance, sinkage and trim are calculated. Subsequently, the collocation points are moved to the updated free surface. Then the difference between the normal velocity through the free surface and the atmospheric pressure is calculated. This should be below a predefined tolerance. If this is not the case, the source strengths are calculated again until convergence is obtained.

As mentioned, the wave making resistance is calculated in two different ways. The first method ( $Rw1$ ) uses pressure integration from the hull. A disadvantage of this method is that it is quite sensitive to the hull panelling. Small changes in the panel lay-out of the hull can lead to large differences in the value for the wave making resistance. However, the wave pattern is much less sensitive to the panel distribution. Therefore the wave making resistance is also computed with a wave cut analysis, resulting in the  $Rw3$  value (Raven and Prins, 1998). This value can be obtained from the dispersion relation and two wave amplitudes. These amplitudes can be found by applying Fourier analysis of the wave height distribution along at least two transverse cuts behind the ship. Applying more cuts increases the accuracy of the result. RAPID uses eight transverse cuts. The longitudinal position of the wave cuts

strongly influences the result. To eliminate variations, the wave cuts are spread over a wave length. Though the  $Rw3$  value is less sensitive for the panel lay-out on the hull, it is affected by numerical damping. This usually leads to smaller absolute values of the wave making resistance than the pressure integration method. Therefore, the  $Rw3$  is more suitable for comparative research than for absolute resistance predictions. This suggests that the  $Rw3$  value is the most adequate value to use in this research.

### 4-3-2 Grid generation

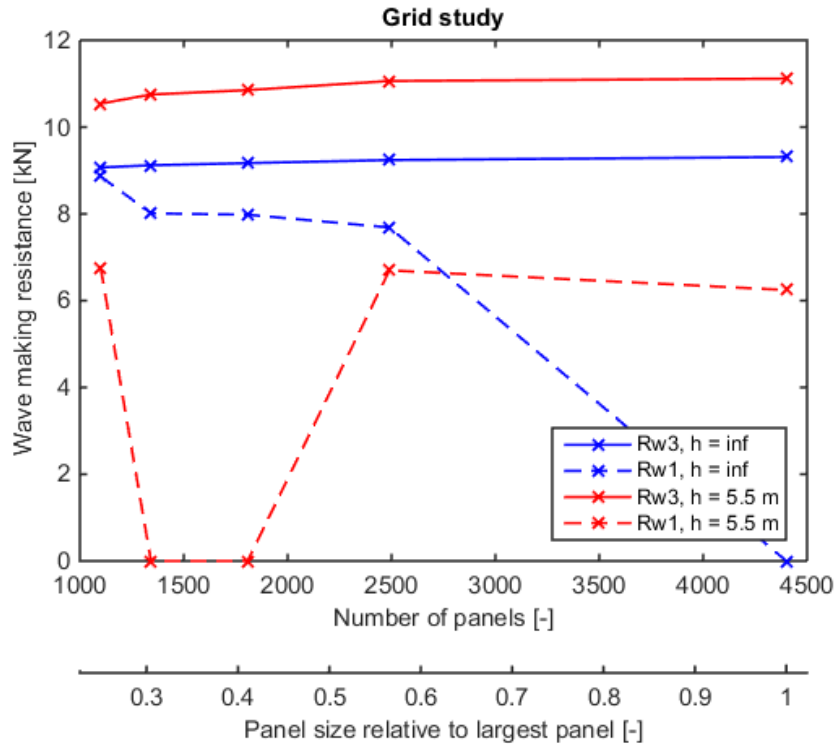
For each combination of Froude number, water depth and bow shape, a potential flow calculation is carried out to calculate the wave making resistance. In total, this results in 1064 calculations. Before the calculations can be carried out, grids have to be constructed for the different shapes. This has been programmed in Python such that it can be done automatically. Separate grids are constructed for the bow, the parallel midship and the stern. Afterwards, the grids are connected and oriented into the coordinate system of RAPID. According to the RAPID manual the total hull grid has to be constructed of at least 1500 panels for an accurate calculation (MARIN, 2015b). However, the running time for RAPID is not critical, so a larger number of panels can be applied without resulting in excessive computation times. An advantage of a larger amount of panels is that the curvature of the surface in the bow can be modelled more precisely. For the bow, a high grid resolution has been applied, since this is the region of interest where the wave making occurs. The grids of the parallel midship and the stern are constructed with a lower resolution.

A short grid study has been carried out to determine the minimum required numbers of panels. Five different grids ranging from coarse to fine are produced for a ship consisting of a bow, a parallel midship and a stern. The stern has the shape of a Wigley hull to minimise the impact on the wave pattern. Each grid has a different number of panels. An overview of this is given in Table 4-6. For each grid the  $Rw1$  and  $Rw3$  values are calculated for  $Fn = 0.14$  at two water depths: infinite and 5.5 m.  $Fn = 0.14$  and  $h = 5.5$  m are representative conditions for the experiments that will be carried out. The results of the grid study are presented in Figure 4-8. It can be observed that the number of panels does not influence the value of  $Rw3$  significantly. Several  $Rw1$  values turn out to be zero. According to the output file of RAPID this is due to the immersed transom. This is an unexpected result, since the stern has the shape of a Wigley hull and does not have a transom at all. Numerical errors are likely to be the cause for this situation. This problem did not only occur in the grid study, but also during the experiments. Paragraph 5-1-1 elaborates further on this. For the moment it seems that  $Rw3$  is indeed the most adequate measure for the wave making resistance. The number of panels is not normative for the computation time and can be increased if wanted. Therefore, the number of panels for the experiments is set well above the guideline of 1500 panels. An overview of the number of grid panels for the experiments is given in Table 4-7. To prevent submerged contours, the hull has been enlarged in vertical direction to a depth of 8.0 m. The depth of the real hull is 5.0 m. Similar to the stern in the geometry, the stern of the experiments has the shape of a Wigley hull.

A batch script is used to run the calculations automatically. Several additional input settings are required. These are presented in Table 4-8. The number of panels per wave length and

**Table 4-6:** Number of panels for the five cases of the grid study

	Coarse			Fine	
<b>Stern</b>	300	374	507	690	1200
<b>Midship</b>	600	726	975	1350	2400
<b>Bow</b>	200	242	325	450	800
<b>Total</b>	<b>1100</b>	<b>1342</b>	<b>1807</b>	<b>2490</b>	<b>4400</b>

**Figure 4-8:** Results of grid study

number of strips in the width of the domain are somewhat reduced compared to the default settings. This is because the solution does not converge with the default number of panels for several cases. This is because the local steepness of a wave exceeds the maximum steepness value. With a lower number of panels, the waves are flattened out, resulting in a lower steepness. The number of panels may not be decreased too much, otherwise a proper physical representation of the wave is not possible any more. The minimum recommended number of panels per waves is 20 (MARIN, 2015b). The setting for the experiments complies with this recommendation. After the input settings are defined, the calculations are carried out. The output of the calculations consists of files containing information about the pressures, velocities, forces and wave elevations. Furthermore, output files for the visualization of the results are generated. The computational time for all 133 bows varies between 12 hours (for the highest Froude numbers) and 18 hours (for the lowest Froude numbers). In total, a week was needed to complete all calculations.

**Table 4-7:** Number of grid panels for the hull

Segment	No. of columns	No. of rows	No. of panels
Bow	60	80	4800
Midship	50	30	1500
Stern	30	30	900
<b>Total</b>			<b>7200</b>

**Table 4-8:** Settings for RAPID calculations

Parameter	Input
Calculation mode	Automatic
Max. no. of iterations	50
Convergence criterion	0.0002
No. of panels per wavelength	25
No. of strips for half width of domain	25

#### 4-4 Viscous flow calculations

In Section 4-3 several reasons are given for why the main focus of this research lies on calculating the wave making resistance with potential flow calculations. However, this does not mean that the bow is not subjected to viscous forces. In absolute values the viscous forces are even expected to be much higher than the wave making forces, since the Froude numbers are low. Viscous forces on the bow can occur in particular on the transition between the bottom and the sides of the bow. The sharper this transition is, the larger the pressure gradients will be, resulting in a higher viscous pressure resistance. Furthermore, the different bow shapes may lead to different wetted areas, resulting in different values for the viscous plate friction. Experiments have to be carried out to identify how large these viscous effects are. The expectation is that these effects are rather similar for the different bow shapes. Therefore, the goal of the experiments is to check to which extent the viscous resistance changes for different bow shapes rather than estimating the absolute value of the viscous resistance.

Viscous effects can not be calculated with RAPID, so different software has to be used. CFD codes are suitable for this type of calculations. PARNASSOS and ReFRESCO are two CFD codes that are developed at MARIN and are dedicated to and optimised for ship applications (see Section 3-3). Another commonly used code is Fluent. This is a more generic code that is also suited for other fluid mechanics applications. Since the hull forms that are considered in this research do not have complex shapes or appendages, it does not matter which CFD code is used. For this research PARNASSOS is chosen. This is mainly for practical reasons: it was already available and an experienced user could be consulted for executing the calculations. Raven gives an overview of the characteristics of PARNASSOS and its use in a shallow water situations (Raven, 2012), which are now described here. PARNASSOS predicts the steady flow around ship hulls with a RANS solver. The full coupled momentum and continuity equations are used to ensure incompressibility. The grid consists of multiple blocks. Finite difference discretisation is used. The domain is decomposed in subdomains, in which the velocity and pressure values are computed. The domains are addressed one by one until convergence is

**Table 4-9:** Parameters for bows for viscous calculations,  $Rw3$  in kN and  $Awet$  in  $m^2$ 

Bow	Lbow	$\nabla$	$\alpha$	$\beta$	Cwp	SAC25	SAC75	T25	Rw3	Awet
<b>11</b>	0.528	0.489	0.603	0.178	0.399	0.530	0.406	0.450	11.22	1660
<b>14</b>	0.939	0.617	0.916	0.106	0.904	0.134	0.426	0.591	7.65	1667
<b>26</b>	0.336	0.652	0.359	0.212	0.469	0.396	1.000	0.737	5.71	1670
<b>90</b>	0.888	0.399	0.331	0.833	0.378	0.369	0.328	0.560	8.46	1656

obtained. The solver is rather insensitive to the mesh aspect ratio. It is robust and a high numerical accuracy can be obtained within a reasonable amount of time (several hours to one day). In practice PARNASSOS is used e.g. for analysing the flow around the ship, predicting the wake field and computing the free-surface viscous flow, for both model scale and full scale. For shallow water resistance predictions there are several additional requirements. A boundary condition at the waterway bottom has to be imposed. This condition states that the flow has no slip relative to the bottom. The bottom moves relative to the ship with the sailing speed of the ship. The shape of the domain is slab-like for shallow water calculations. The boundary condition for the lateral boundary is derived from a potential flow calculation. There is a strong contraction of the grid towards the hull.

Since these experiments are carried out only to check the assumption that the viscous resistance does not change significantly for the different bow shapes, the number of experiments is limited. This is also for practical reasons. While the potential flow calculations in RAPID are in general finished within minutes, viscous calculations with PARNASSOS usually take several hours to a day to converge. Therefore calculations are carried out for only one Froude number and water depth:  $Fn = 0.14$  and  $h = 5.5$  m. These are the medium Froude number and medium water depth. This situation is deemed representative, because the Froude depth number is high enough for encountering shallow water effects, but not so high that extreme shallow water effects or numerical problems are likely to occur. Four bows are selected for the viscous calculations. The bow shape parameters of these bows are scattered over the design space. Since viscous effects are largely dominated by the wetted area, double body flow calculations are carried out. Including free surface waves does not lead to a significant change of the wetted area. For example: a typical wetted area for a free surface obtained from RAPID is  $1678 m^2$  for the entire ship. The wetted area up to the still waterline for the same ship is  $1675 m^2$ . The difference is so small that the plate friction does not increase significantly when a free surface is included. An overview of the different bow shape parameters of the four bow shapes is given in Table 4-9. The parameters are normalised between 0 (for the lowest value of the entire data set) and 1 (for the highest value of the entire dataset) to obtain a quick insight in the scatter of the parameters over the design space. For reference, the  $Rw3$  values from RAPID and the total wetted area up to the still waterline are also presented in that table. It can be seen that the wetted areas are rather similar for all ships.

In general, it takes some time to get acquainted with PARNASSOS or other software for numerical resistance prediction methods. Since the focus of this research is on the wave making resistance and not on the viscous calculations described here, the actual execution of the calculations was outsourced. More details on e.g. the mesh generation and the input settings are therefore not reported in this thesis. The results of the calculations are returned

in the form of viscous resistance coefficients. Section 5-2 elaborates on the results of these calculations.

---

# Chapter 5

---

## Results

This chapter elaborates on the results of the experiments that are described in Chapter 4. Section 5-1 focusses on the the results of the potential flow calculations. In Section 5-2 the results of the viscous flow calculations are discussed.

### 5-1 Potential flow calculations

This section elaborates on the results of the potential flow calculations. First, it is described in Paragraph 5-1-1 how the wave making resistance is retrieved from the experiments described in Chapter 4. Subsequently, Paragraph 5-1-2 elaborates on how linear models are generated to examine the results. Paragraph 5-1-3 elaborates on the practical application of the statistical analysis.

#### 5-1-1 Wave making resistance

RAPID calculations have been carried out for all 133 bows shapes for the eight combinations of Froude numbers and water depths. As mentioned in Paragraph 4-3-1, the wave making resistance is calculated in two different ways. This paragraph also explains why the  $Rw3$  value, which is obtained from analysing transverse cuts through the waves behind the stern, seems to be the most suitable value for comparing different geometries. Both values for the wave making resistance are plotted in Figure 5-1 for the different Froude numbers and water depths. It can be observed that there is a linear relation between the two values. The absolute  $Rw1$  values are smaller than the  $Rw3$  values. This is remarkable, since usually the  $Rw3$  values are smaller due to numerical damping (see Paragraph 4-3-1). For low  $Rw3$  values, the  $Rw1$  values even become so small that a negative value is obtained. This is not a physical realistic situation. The RAPID output files are examined in order to find the cause of this non-physical phenomenon. The  $Rw1$  value is computed from a non-dimensionalised total force coefficient. It turns out that this total force coefficient is negative, leading to a negative resistance value. The total force coefficient is the sum of the force coefficients of all strips. The output files also

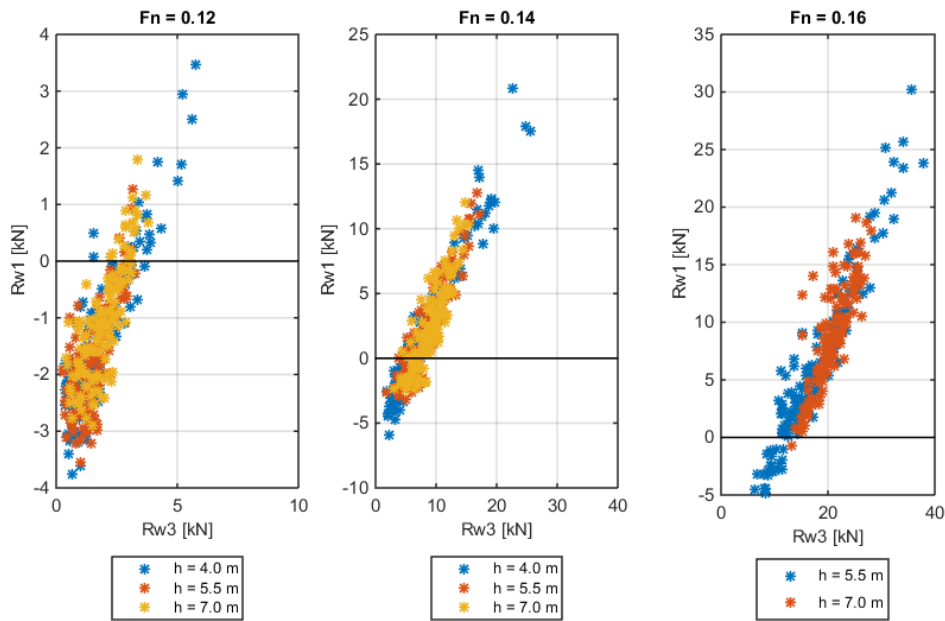


**Figure 5-1:** Rw1 and Rw3 values for different Froude numbers and water depths

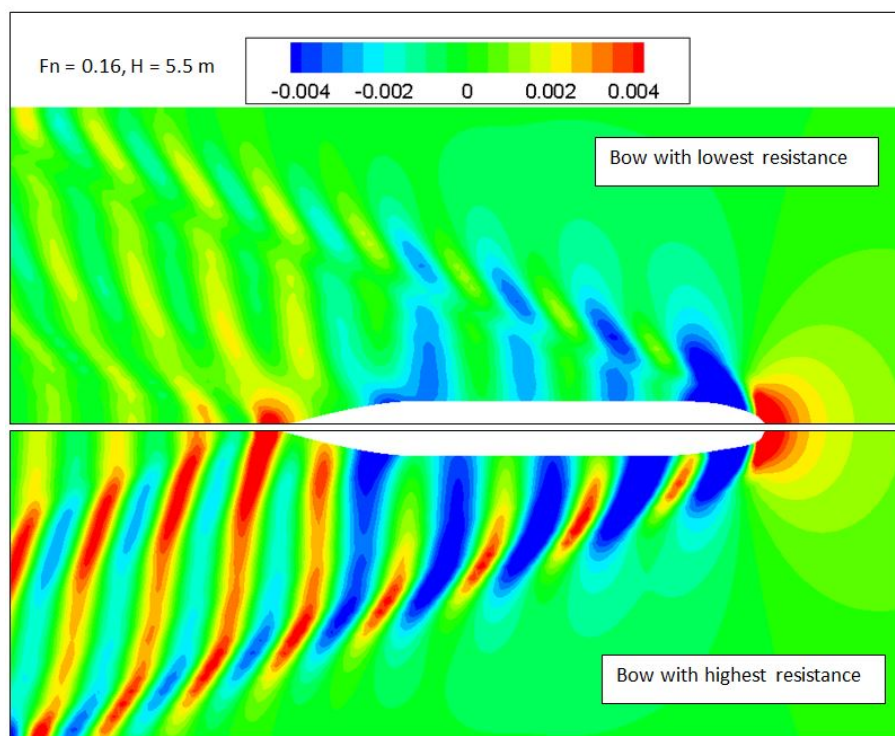
give the subtotals of these force coefficients for the bow, the midship and the stern. For the midship the subtotal of the force coefficients is practically zero, which is physically realistic because this part barely has a normal component in the longitudinal direction. For the bow, the subtotal is positive and for the stern the subtotal is negative. This is physically realistic. However, the negative force coefficient for the stern outweighs the positive force coefficient of the bow, leading to a negative total force coefficient. Hence, it seems that the negative force on the stern is overestimated by the program. As mentioned in Section 3-3, panel codes are in general not able to predict the stern wave profile accurately due to the neglect of viscosity. This leads to overestimated stern wave profiles. It is expected that this is the source of the negative Rw1 values that are obtained in the experiments.

Though the absolute values of Rw1 are unreliable, the relation between Rw1 and Rw3 is linear. This indicates that the trends are captured well. Rw3 still seems a suitable value to use to compare the different bow shapes. This can be confirmed further by having a look at the mathematical representation of the relation between the two values. This relation can be represented by a linear regression line. The coefficients for the lines for each situation along with the  $R^2$  values are presented in Table 5-1. As can be observed in this table, the  $a$ -coefficient, which represents the ratio between the Rw1 and Rw3 values, is practically 1 for all cases. This indicates that both values are on average equal, but with a shift of the zero point. This shift is represented by the  $b$ -coefficient. High Froude numbers lead to higher resistances and hence lower  $b$ -coefficients. From a physical point of view the negative Rw1 values do not make sense, but the trends are captured well, so it seems that Rw3 is also an adequate value to measure the wave making resistance.

Since the wave making resistance is computed from the wave profile behind the ship, the Rw3 value can only be used if no interaction with the stern wave system occurs. This can

**Table 5-1:** Coefficients for relations between  $Rw1$  and  $Rw3$  for the relation  $y = ax + b$ 

$F_n$	$h$ [m]	$a$	$b$	$R^2$
0.12	4.0	0.99	-3.16	0.80
0.12	5.5	0.96	-3.14	0.58
0.12	7.0	1.00	-3.03	0.63
0.14	4.0	0.98	-5.89	0.95
0.14	5.5	1.02	-6.39	0.87
0.14	7.0	1.12	-7.60	0.78
0.16	5.5	1.01	-11.50	0.92
0.16	7.0	0.96	-10.90	0.64

**Figure 5-2:** Normalised wave heights for bow shapes with the highest and lowest  $Rw3$  values for  $F_n = 0.16$  and  $h = 5.5$  m

be checked visually. In Figure 5-2, two wave profiles are presented for the case where  $F_n = 0.16$  and  $h = 5.5$  m. The wave profile on the top is for the bow shape resulting in the lowest value for  $Rw3$ . The bottom wave profile is for the bow shape that results in the highest value for  $Rw3$ . The wave heights are normalised with the ship length. A clear difference between the two wave patterns can be observed. The wave pattern consists of both divergent and transverse waves. The divergent waves from the bow move away from the ship with the Kelvin angle. The transverse waves move in the longitudinal direction of the ship. At the stern, a second wave pattern with a Kelvin angle can be observed. Since the divergent waves from the bow move away from the ship, those waves do not interfere with the stern wave system. The transverse waves could interfere with the stern wave system, but only within

the Kelvin wedge at the stern. It can be observed that the wave systems in the Kelvin wedge are slightly different. In the bottom part of the figure, the wave heights are larger than in the top part. However, the interference is not severe and covers only a small part of the wave system. Therefore it is not likely that the trends of the influence of the bow shape are significantly influenced by the interaction. Apart from the small interaction, two other effects can be observed:

1. Longitudinal wave positions. Wave crests and troughs can be observed along the ship. The troughs are most clearly visible. There is a difference in the longitudinal positions of the troughs. For the top situation, the bow length is smaller. Therefore, the trough in the bow wave system is followed immediately by the trough that is created at the forward shoulder. Subsequently, the following troughs are located more forward than in the bottom situation. This indicates that the bow length has a substantial influence on the wave pattern.
2. Wave heights along the hull. As mentioned in point 1, the wave troughs are clearly visible along the hull. Behind the ship, the wave crests are clearly visible. This confirms that sinkage occurs due to the limited water depth.

Due to the second effect, the height of the wave crests at the stern is exaggerated. This should not be confused with interaction between the bow wave system and the stern wave system.

More information on the values of  $Rw_3$  can be obtained by plotting the average value for the different Froude numbers and water depths. This is given in Figure 5-3. Although individual bow shapes may have various resistance characteristics, the expected general trend is that higher Froude numbers and lower water depths lead to higher values for  $Rw_3$ . As can be observed in the figure, this applies partially to the obtained  $Rw_3$  values. Lower Froude numbers lead indeed to lower  $Rw_3$  values. However, the effect of the different water depths is not entirely as expected. For  $Fn = 0.16$ , a water depth of 7.0 m leads on average to higher  $Rw_3$  values than a water depth of 5.5 m. For  $Fn = 0.12$ , the influence of the water depth on the  $Rw_3$  value is not clear as well. Low Froude numbers can be problematic for resistance calculations and furthermore the computation of  $Rw_3$  is sensitive for high Froude numbers. Therefore, the  $Rw_3$  value is inaccurate as a measure for the absolute value of the wave making resistance. It is therefore not desired that the bow shapes are compared *between* the different Froude numbers and water depths. Therefore the bow shapes will only be compared *within* the different combinations of Froude numbers and water depths.

An alternative method has been tried to obtain the wave making resistance of the bow. In this method, the bow was isolated from the rest of the ship to completely filter out eventual interactions between the bow wave system and the stern wave system. Furthermore, this method was expected to give a better estimate of the absolute value of the wave making resistance. Unfortunately, this method has not led to usable results. A description of this method is given in Appendix A. The  $Rw_3$  values remain the used values for the analysis of the influence of the bow shape on the wave making resistance.

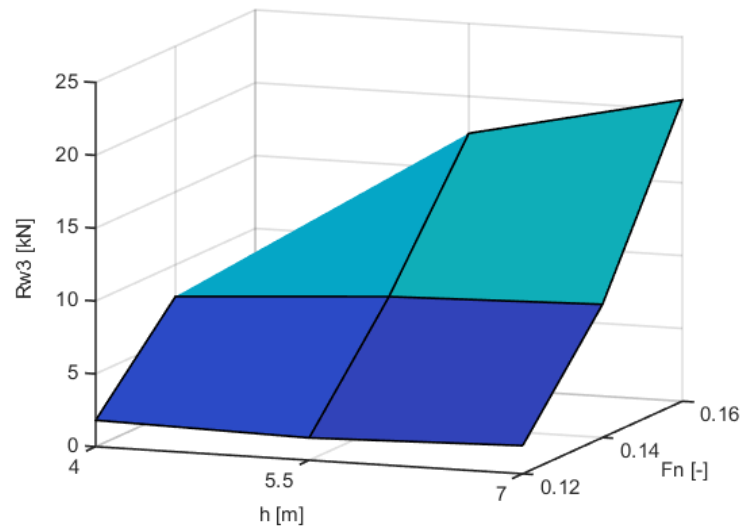


**Figure 5-3:** Mean  $Rw3$  value of all bow shapes for different Froude numbers and water depths

### 5-1-2 Linear model generation

The influence of the bow shape parameters on the  $Rw3$  values can be determined with statistical analysis. Linear regression models are used for this. Such models are useful and widely employed for describing relations between parameters in a simple but powerful way. Since multiple parameters are considered to estimate one response variable, the multiple linear regression model is used. Several steps are taken to obtain such a model and to examine its quality. Only the bow shape parameters are included in the regression model. The Froude number and water depth are not included, since the  $Rw3$  values are useful for comparing different geometries, but less useful for predicting the actual value of the wave making resistance (see Section 5-1-1). Eight separate linear regression models are made for the different combinations of Froude numbers and water depths. The way in which the linear regression models are obtained is described here for the case where  $Fn = 0.12$  and  $h = 7.0$  m. For the other cases, the same procedure is followed. The statistical analysis is carried out with MATLAB. The online MATLAB documentation about linear regression was used as a basis for the statistical analysis (MathWorks Documentation, 2016).

A requirement for the construction of a linear regression model is that the evaluated parameter has a normal distribution (Ledolter and Hogg, 2010). Therefore, it is determined first whether this is the case. This is done by constructing a histogram of the  $Rw3$  values, which is presented in Figure 5-4. It can be seen that the values of  $Rw3$  are indeed normally distributed, with a mean around 2.0 kN. This means that the data can be used for constructing a linear regression model.

Subsequently it is determined which of the eight bow shape parameters should be included in the model. It is likely that some parameters contribute more to the wave making resistance than others. To get a first insight in this, several linear models are constructed with four of the eight parameters. Interactions and quadratic terms are included. For each combination

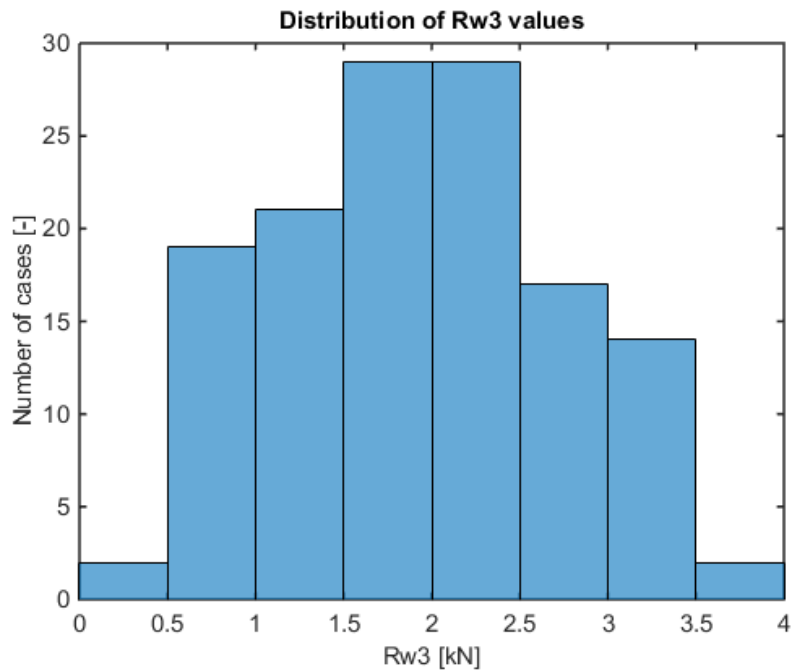


**Figure 5-4:** Distribution of  $Rw3$  for  $Fn = 0.12$ ,  $h = 7.0$  m

**Table 5-2:**  $R^2$  values for different combinations of parameters

Lbow	$\nabla$	$\alpha$	$\beta$	Cwp	SAC25	SAC75	T25	$R^2$
x	x	x	x					0.784
x	x				x	x		0.976
				x	x	x	x	0.657
		x	x			x	x	0.761
		x		x	x	x		0.916

of parameters, the  $R^2$  value for the associated model is computed. The higher the  $R^2$  value is, the better the model represents the  $Rw3$  data. A few examples are presented in Table 5-2. It can be observed that the combination of the bow length, the ship volume and the slope of the sectional area curves at 25% and 75% of the bow length leads to the highest  $R^2$  value, thus the best prediction of  $Rw3$ . Many more combinations of parameters exist, but they do not lead to higher  $R^2$  values.

The bow length, ship volume and slopes of the sectional area curves are used for further refinement of the linear model. Interactions and quadratic terms are still included. However, some interactions or quadratic terms may not contribute significantly to the linear model. A measure for the significance of the different terms in the model is the p-value. This value is defined as the probability of obtaining a result equally or more different from the result specified by the null hypothesis, assuming that the null hypothesis is true (Lane, 2016). The null hypothesis in general states that a parameter is zero or that the difference between parameters is zero. In this case the null hypothesis states that the obtained value for the wave making resistance is the same for each term in the model. A small p-value ( $\leq 0.05$ )

**Table 5-3:** Coefficients and p-values for the linear model

Term	Coefficient	p-value
(Intercept)	-83.671	0.93811
<i>Lbow</i>	-7.9116	0.42736
$\nabla$	0.24519	0.70563
<i>SAC25</i>	-325.15	0.063055
<i>SAC75</i>	-206.07	8.70E-06
<i>Lbow</i> · $\nabla$	0.00078865	0.78856
<i>Lbow</i> · <i>SAC25</i>	1.5095	0.07193
<i>Lbow</i> · <i>SAC75</i>	1.4212	5.19E-10
$\nabla$ · <i>SAC25</i>	0.079093	0.12903
$\nabla$ · <i>SAC75</i>	0.048895	0.00041129
<i>SAC25</i> · <i>SAC75</i>	33.657	4.45E-16
<i>Lbow</i> <sup>2</sup>	0.0727	0.0051928
<i>Vship</i> <sup>2</sup>	-6.03E-05	0.53906
<i>SAC25</i> <sup>2</sup>	33.596	5.24E-06
<i>SAC75</i> <sup>2</sup>	8.703	6.46E-26

**Table 5-4:** P-values for the ANOVA

Term	p-value
<i>Lbow</i>	3.78E-63
$\nabla$	3.87E-30
<i>SAC25</i>	3.26E-45
<i>SAC75</i>	3.06E-87
<i>Lbow</i> · $\nabla$	0.78856
<i>Lbow</i> · <i>SAC25</i>	0.07193
<i>Lbow</i> · <i>SAC75</i>	5.19E-10
$\nabla$ · <i>SAC25</i>	0.12903
$\nabla$ · <i>SAC75</i>	0.00041129
<i>SAC25</i> · <i>SAC75</i>	4.45E-16
<i>Lbow</i> <sup>2</sup>	0.0051928
<i>Vship</i> <sup>2</sup>	0.53906
<i>SAC25</i> <sup>2</sup>	5.24E-06
<i>SAC75</i> <sup>2</sup>	6.46E-26

indicates that the null hypothesis can be rejected, i.e. that the associated term is statistically significant. The value 0.05 is the conventional value to determine whether the null hypothesis can be rejected. Other values can be used as well, but for this research the value 0.05 was used because this is traditionally the most common value to use. Table 5-3 gives the coefficients and p-values for the different terms in the model. The significant terms are coloured red. However, these results could still be the result of chance. Therefore it is needed to examine the quality of the model. This can be done with an analysis of variance (ANOVA). This method also gives a p-value. These are presented in Table 5-4. The p-values for the ANOVA are different from the p-values of the linear model. As can be seen in the ANOVA, the

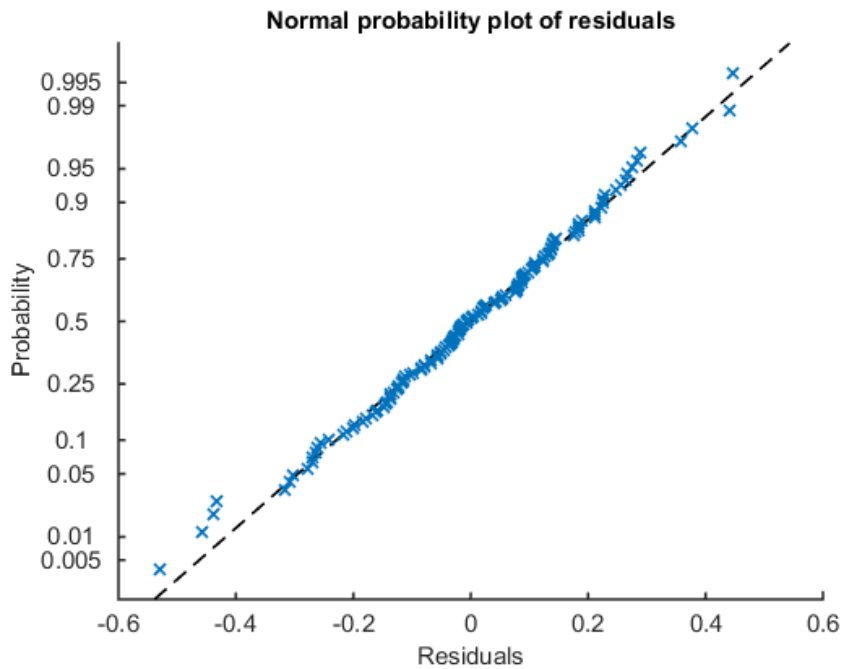


**Figure 5-5:** Normal probability plot for  $Rw3$  residuals for  $Fn = 0.12$  and  $h = 7.0$  m

contribution of the individual parameters is very significant. Furthermore, almost every  $p$ -value in the table is equal or less than 0.05. A balance has to be found between the amount of terms taken into account in the model and the accuracy of the model. The accuracy increases slightly with more terms, but in general it is desired that the model is kept as simple as possible. If too many terms are included in the model, it is difficult to relate the model to the underlying physical phenomena. For this case it has been determined that the four most important interactions and quadratic terms are taken into account. The other six interactions and quadratic terms are left out of the model, since the increase in accuracy is limited. The obtained  $R^2$  value with this adjusted model is 0.947.

For further examination of the quality of the fitted model, the residuals can be plotted. The residual is defined as the difference between the observed value (in this case a single  $Rw3$  value) and the sample mean (in this case the mean of all  $Rw3$  values for which  $Fn = 0.12$  and  $h = 7.0$  m). A common way to present the residuals is with a probability plot. This is given in Figure 5-5. The plot shows how the distribution of the residuals compares to a normal distribution with matched variance. As can be observed, the residuals fit well to the normal distribution. No obvious outliers can be observed. Outliers usually have a large unwanted impact on the fitted model. In cases where outliers are present, they can be identified with this plot type. Subsequently, they can be excluded from the model to obtain a better model.

Since the normal probability plot indicates that no additional adjustments to the model are needed, the fitted model can be used to estimate the wave making resistance for the different bow shapes. Ideally, these estimates would be similar to the  $Rw3$  values that are obtained from the experiments. Figure 5-6 shows the  $Rw3$  values and the wave making resistance as

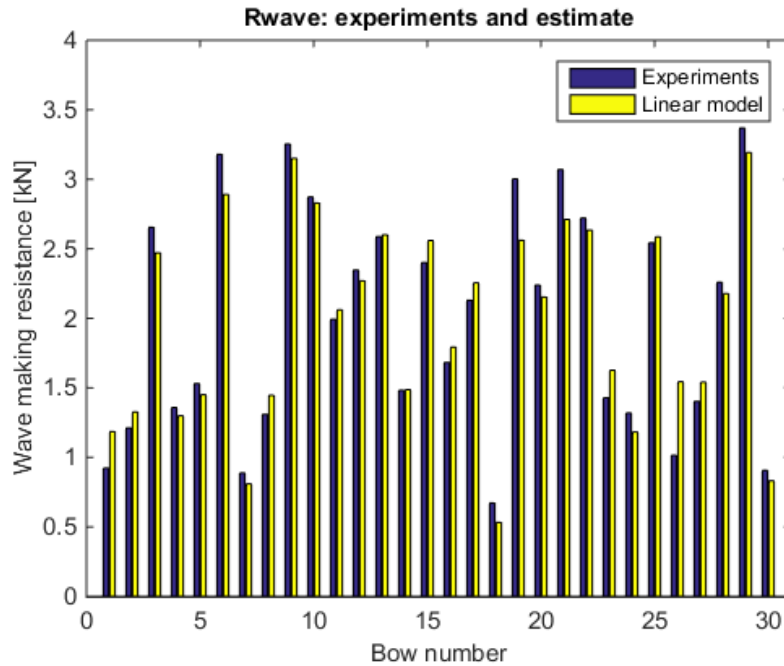


**Figure 5-6:** Comparison of  $R_{w3}$  values and fitted model for  $Fn = 0.12$  and  $h = 7.0$  m

**Table 5-5:** Overview of final model for  $Fn = 0.12$  and  $h = 7.0$  m

Term	Coefficient	p-value
(Intercept)	112.2	8.41E-31
$L_{bow}$	-1.1492	1.46E-24
$\nabla$	-0.020789	3.76E-20
$SAC_{25}$	-46.479	1.52E-39
$SAC_{75}$	-39.897	4.06E-22
$L_{bow} \cdot SAC_{75}$	0.48732	1.48E-08
$SAC_{25} \cdot SAC_{75}$	26.078	2.14E-32
$SAC_{25}^2$	21.196	1.85E-25
$SAC_{75}^2$	8.3428	2.66E-21

estimated with the fitted model. For visibility reasons, only thirty bow shapes are included in the graph. The other bow shapes show a similar behaviour. The trends in the resistance are captured reasonably well with the fitted model. For high resistance values, the fitted model seems to underestimate the resistance slightly. For some individual bow shapes a large deviation between the experiments and the fitted model is found, such as for bow shape 26 in the figure. The relative deviation between the experiments and the fitted model for all bow shapes is plotted in Figure 5-7. In 89% of the cases the deviation is smaller than 20%. In 71% of the cases the deviation is smaller than 10%. The coefficients and p-values of the final model are presented in Table 5-5.

Up to this point, the described statistical analysis applies to the case where  $Fn = 0.12$  and  $h = 7.0$  m. For the other seven combinations of Froude numbers and water depths, the same

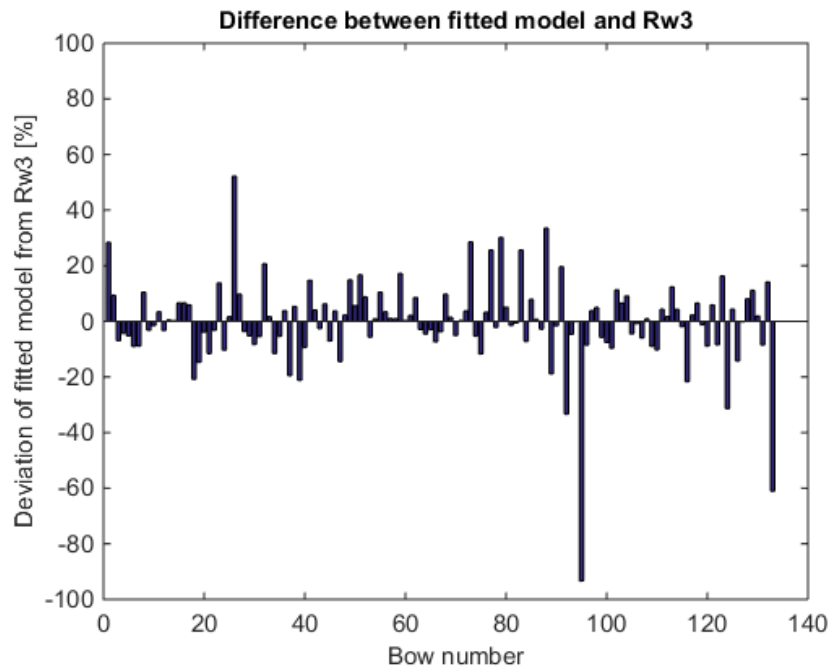


**Figure 5-7:** Deviations between fitted model and experiment for  $Fn = 0.12$  and  $h = 7.0$  m

procedure is followed. The resulting linear models are presented in Table 5-6. The associated statistical plots are presented in Appendix B. Several interesting aspects can be observed in Table 5-6. For  $h = 4.0$  m no results are obtained. This is because the  $Rw3$  values for  $Fn = 0.12$  and  $Fn = 0.14$  at that water depth are not distributed normal. Therefore, no regression analysis can be carried out. For the other water depths it is possible to generate an adequate linear model. The models are much like the model explained in Table 5-5. For all situations, the bow length, ship volume and slopes of the sectional area curve are the best parameters for describing the wave making resistance, i.e. the parameters leading to the highest  $R^2$  value. It differs per situation which interaction terms and quadratic terms are included. For  $Fn = 0.16$  and  $h = 7.0$  m, the obtained  $R^2$  value is somewhat lower. This model does not include the slope of the sectional area curve at 75% of the bow length. Including this term does not lead to a substantial higher  $R^2$  value.

It would be interesting to investigate whether some of the parameters in the obtained linear models may have more or less influence when the Froude number or water depth changes. This can be investigated by analysing the coefficients of the terms in the model. However, it is not possible to compare the coefficients that can be seen in Table 5-6 directly. For example: magnitude of the ship volume (about  $2900 [m^3]$ ) is much larger than the magnitude of the bow length (about  $20 [m]$ ). Therefore, the coefficient for the ship volume is smaller than the coefficient for the bow length. This principle holds for all terms in the models. Furthermore, the coefficients are related strongly to the value of the intercept. For statistical reasons it is not desirable that the intercept is left out of the model (The Minitab Blog, 2016). This problem can be overcome by generating the same linear models again, but with normalised values for the parameters and the  $Rw3$  values. These are normalised by subtracting the

**Table 5-6:** Linear models with coefficients for different Froude numbers and water depths

<b>Fn   h [m]</b>	<b>4.0</b>	<b>5.5</b>		<b>7.0</b>			
<b>0.12</b>	Non-normal distribution	(Intercept)	111.76	See Table 5-5			
		<i>Lbow</i>	-1.3943				
		$\nabla$	-0.0186				
		<i>SAC25</i>	-47.114				
		<i>SAC75</i>	-49.659				
		<i>Lbow</i> · <i>SAC75</i>	0.77264				
		<i>SAC25</i> · <i>SAC75</i>	27.386				
		<i>SAC25</i> <sup>2</sup>	22.784				
		<i>SAC75</i> <sup>2</sup>	10.43				
		<i>R</i> <sup>2</sup>	0.956				
<b>0.14</b>	Non-normal distribution	(Intercept)	-415.39	(Intercept)	-296.36		
		<i>Lbow</i>	9.2299	<i>Lbow</i>	5.776		
		$\nabla$	0.11009	$\nabla$	0.082		
		<i>SAC25</i>	38.509	<i>SAC25</i>	27.418		
		<i>SAC75</i>	-24.32	<i>SAC75</i>	-9.2606		
		<i>Lbow</i> <sup>2</sup>	-0.197	<i>Lbow</i> <sup>2</sup>	-0.1268		
		<i>SAC75</i> <sup>2</sup>	7.4826	<i>SAC75</i> <sup>2</sup>	0.66315		
		<i>R</i> <sup>2</sup>	0.957	<i>R</i> <sup>2</sup>	0.941		
		<b>0.16</b>	N/A	(Intercept)	-1174.4	(Intercept)	-1545.9
				<i>Lbow</i>	2.0356	<i>Lbow</i>	862.38
$\nabla$	0.39676			$\nabla$	942.94		
<i>SAC25</i>	-137.6			<i>SAC25</i>	716.1		
<i>SAC75</i>	-91.826			<i>Lbow</i> · $\nabla$	11.937		
<i>Lbow</i> · <i>SAC25</i>	13.286			<i>Lbow</i> · <i>SAC25</i>	189.84		
<i>SAC25</i> · <i>SAC75</i>	-41.174			$\nabla$ · <i>SAC25</i>	9.1083		
<i>SAC75</i> <sup>2</sup>	46.921						
<i>R</i> <sup>2</sup>	0.972			<i>R</i> <sup>2</sup>	0.898		

mean and dividing by the standard deviation, such that the mean is 0 and the variance is 1. The advantage of this method is that the intercept is close to zero, which makes it easier to compare the different models. These altered models are presented in Table 5-7. The terms with the highest coefficients are highlighted in red. These coefficients have the most influence on the wave making resistance. For  $Fn = 0.12$ , the bow length has the highest coefficient. For  $Fn = 0.14$ , the slope of the sectional area curve at 25% of the bow length turns out to have the largest effect on the resistance. For  $Fn = 0.16$ , the bow length, ship volume and slope of the sectional area curve at 25% of the bow length all seem to be more or less equally important. The differences between results for the two water depths are small, except for  $Fn = 0.16$ . The coefficients in this model have a higher magnitude, indicating an stronger influence on the wave making resistance. The interaction terms and quadratic terms do not have a large influence on the wave making resistance.

An important aspect of statistical analysis is evaluating how the results relate to the underlying physics. Sections 3-1 and 3-2 elaborate on why the bow length, ship volume and slope

**Table 5-7:** Normalised coefficients for linear models

<b>Fn   h [m]</b>	<b>5.5</b>		<b>7.0</b>	
<b>0.12</b>	(Intercept)	-0.324	(Intercept)	-0.289
	<i>Lbow</i>	<b>-1.532</b>	<i>Lbow</i>	<b>-1.500</b>
	∇	-0.618	∇	-0.650
	<i>SAC25</i>	-0.942	<i>SAC25</i>	-1.084
	<i>SAC75</i>	-1.214	<i>SAC75</i>	-1.314
	<i>Lbow:SAC75</i>	0.338	<i>Lbow:SAC75</i>	0.200
	<i>SAC25:SAC75</i>	0.689	<i>SAC25:SAC75</i>	0.616
	<i>SAC25</i> <sup>2</sup>	0.306	<i>SAC25</i> <sup>2</sup>	0.267
	<i>SAC75</i> <sup>2</sup>	0.492	<i>SAC75</i> <sup>2</sup>	0.369
<b>0.14</b>	(Intercept)	0.102	(Intercept)	0.141
	<i>Lbow</i>	0.437	<i>Lbow</i>	0.241
	∇	0.843	∇	0.802
	<i>SAC25</i>	<b>1.189</b>	<i>SAC25</i>	<b>1.080</b>
	<i>SAC75</i>	-0.579	<i>SAC75</i>	-0.590
	<i>Lbow</i> <sup>2</sup>	-0.184	<i>Lbow</i> <sup>2</sup>	-0.151
	<i>SAC75</i> <sup>2</sup>	0.081	<i>SAC75</i> <sup>2</sup>	0.009
	(Intercept)	-0.183	(Intercept)	-0.141
<b>0.16</b>	<i>Lbow</i>	<b>1.520</b>	<i>Lbow</i>	<b>2.177</b>
	∇	<b>1.387</b>	∇	<b>2.129</b>
	<i>SAC25</i>	<b>1.525</b>	<i>SAC25</i>	<b>2.010</b>
	<i>SAC75</i>	-0.391	<i>Lbow:∇</i>	-0.087
	<i>Lbow:SAC25</i>	0.297	<i>Lbow:SAC25</i>	0.416
	<i>SAC25:SAC75</i>	-0.095	∇: <i>SAC25</i>	-0.077
	<i>SAC75</i> <sup>2</sup>	0.262		

of the sectional area curve are important for the resistance. The following observations can be derived from the linear models:

1. Bow length. For the  $Fn = 0.12$  the bow length is the most important parameter. The longer the bow is, the lower the wave making resistance is. This is as expected, since a longer bow leads to a more smooth redirection of the flow around the ship. However, the coefficients for the bow length are positive for the other Froude numbers.
2. Slope of sectional area curve. For the  $Fn = 0.14$ , *SAC25* is the most important parameter. This has to do with the sharpness of the shoulder. The coefficient for this term is positive. This means that a higher slope, i.e. a sharper shoulder, leads to a higher wave making resistance. The relation between *SAC25* and *Rw3* is given in Figure 5-8. This figure confirms the relation found in the linear models. For favourable resistance characteristics, the low value of *SAC25* is combined with a high value for *SAC75*. Therefore, the sign for the coefficients of *SAC75* is negative. This is confirmed in Paragraph 5-1-3, which elaborates on which bow shapes are adequate for practical use. However, the situations where  $Fn = 0.12$  are an exception to this, since both parameters have negative coefficients for this situation.

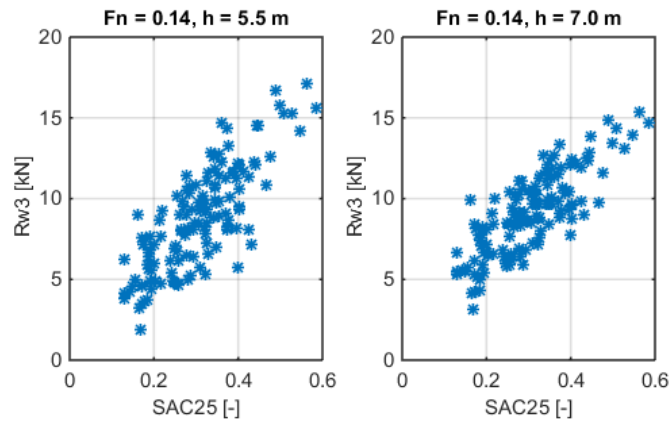


**Figure 5-8:** Relation between  $Rw3$  and  $SAC25$  for  $Fn = 0.14$

It can be concluded that several aspects are in line with the expectations, but that there are exceptions to this. A critical review of the obtained  $Rw3$  values and linear models is therefore needed. Chapter 6 elaborates on this. Furthermore, it is remarkable that the waterline entrance angle is not present in the models. However, this does not directly mean that this parameter is not important, only that the other mentioned parameters are able to predict the wave making resistance more adequately. The rake and ratio between the waterplane areas at 25% and 100% of the draught are also not present in the models. Both parameters describe the bow in vertical direction. This could be a reason for the absence of these parameters in the model, since wave making primary occurs at the surface. The quadratic terms and interaction terms in the model differ per situation. These terms do not directly relate to physical phenomena, but have a more statistical meaning.

### 5-1-3 Practical applications of the linear models

The linear models give a good insight in which parameters have a large influence on the wave making resistance, but do not indicate which bow shapes are adequate for practical use. After all, a good bow shape does not only have minimal resistance, but also a high cargo capacity, as explained in Section 2-1. To get more insight in this, the normalised parameters for the best bows can be listed. First, it has to be determined when a bow shape is defined as "good". Apart from a low resistance, the total ship volume should be as high as possible. Therefore a bow shape is defined as "good" when the ratio of the two parameters is minimised (Equation 5-1). Ideally it would also be included that the sailing speed is as high as possible and the water depth as low as possible. However,  $Rw3$  is suited for comparing the different shapes within a given Froude number and water depth rather than providing the correct absolute value for the wave making resistance. Therefore the best bows are listed per situation.

$$\min \left[ \frac{Rw3}{\nabla} \right] \quad (5-1)$$

An overview of the three best bows per situation is given in Table 5-8. It can be observed that these bows have on average a low slope of the sectional area curve at 25% of the bow length and a high slope at 75% of the bow length. The low slope at 25% of the bow length indicates

**Table 5-8:** Normalised parameter values of best bows per situation

Situation	Bow	Lbow	Vship	$\alpha$	$\beta$	Cwp	SAC25	SAC75	T25
<b>Fn = 0.12</b> <b>h = 5.5 m</b>	92	0.800	0.581	0.300	0.076	0.709	0.077	0.835	0.743
	124	0.912	0.437	0.276	0.208	0.609	0.280	0.624	0.441
	18	0.803	0.693	0.336	0.862	0.730	0.095	0.679	0.853
<b>Fn = 0.12</b> <b>h = 7.0 m</b>	89	0.547	0.843	0.606	0.656	0.830	0.115	0.826	1.000
	92	0.800	0.581	0.300	0.076	0.709	0.077	0.835	0.743
	124	0.912	0.437	0.276	0.208	0.609	0.280	0.624	0.441
<b>Fn = 0.14</b> <b>h = 5.5 m</b>	125	0.226	0.798	0.515	0.591	0.590	0.087	0.955	0.789
	92	0.800	0.581	0.300	0.076	0.709	0.077	0.835	0.743
	43	0.584	0.594	0.403	0.467	0.515	0.110	0.611	0.721
<b>Fn = 0.14</b> <b>h = 7.0 m</b>	125	0.226	0.798	0.515	0.591	0.590	0.087	0.955	0.789
	92	0.800	0.581	0.300	0.076	0.709	0.077	0.835	0.743
	24	0.781	0.531	0.346	0.416	0.623	0.119	0.644	0.510
<b>Fn = 0.16</b> <b>h = 5.5 m</b>	43	0.584	0.594	0.403	0.467	0.515	0.110	0.611	0.721
	24	0.781	0.531	0.346	0.416	0.623	0.119	0.644	0.510
	33	0.324	0.557	0.634	0.167	0.341	0.477	0.601	0.505
<b>Fn = 0.16</b> <b>h = 7.0 m</b>	43	0.584	0.594	0.403	0.467	0.515	0.110	0.611	0.721
	113	0.469	0.514	0.389	0.094	0.431	0.331	0.605	0.401
	100	0.191	0.604	0.767	0.307	0.372	0.582	0.567	0.212
<b>Average</b>		<b>0.643</b>	<b>0.603</b>	<b>0.391</b>	<b>0.348</b>	<b>0.609</b>	<b>0.155</b>	<b>0.725</b>	<b>0.669</b>

**Table 5-9:** Normalised parameter values of poorest bows per situation

Situation	Bow	Lbow	Vship	$\alpha$	$\beta$	Cwp	SAC25	SAC75	T25
<b>Fn = 0.12</b> <b>h = 5.5 m</b>	72	0.756	0.648	1.000	0.392	0.795	0.074	0.297	0.580
	29	0.307	0.542	0.905	0.577	0.264	0.786	0.214	0.316
<b>Fn = 0.12</b> <b>h = 7.0 m</b>	72	0.756	0.648	1.000	0.392	0.795	0.074	0.297	0.580
	107	0.769	0.406	0.837	0.789	0.264	0.503	0.064	0.686
<b>Fn = 0.14</b> <b>h = 5.5 m</b>	65	0.299	0.418	0.821	0.021	0.177	0.950	0.331	0.065
	29	0.307	0.542	0.905	0.577	0.264	0.786	0.214	0.316
<b>Fn = 0.14</b> <b>h = 7.0 m</b>	65	0.299	0.418	0.821	0.021	0.177	0.950	0.331	0.065
	29	0.307	0.542	0.905	0.577	0.264	0.786	0.214	0.316
<b>Fn = 0.16</b> <b>h = 5.5 m</b>	101	0.881	0.330	0.843	0.248	0.457	0.541	0.150	0.230
	109	0.961	0.000	0.392	0.121	0.001	0.735	0.056	0.119
<b>Fn = 0.16</b> <b>h = 7.0 m</b>	89	0.547	0.843	0.606	0.656	0.830	0.115	0.826	1.000
	111	0.605	0.553	0.805	0.620	0.480	0.533	0.329	0.537
<b>Average</b>		<b>0.566</b>	<b>0.491</b>	<b>0.820</b>	<b>0.416</b>	<b>0.397</b>	<b>0.569</b>	<b>0.277</b>	<b>0.401</b>

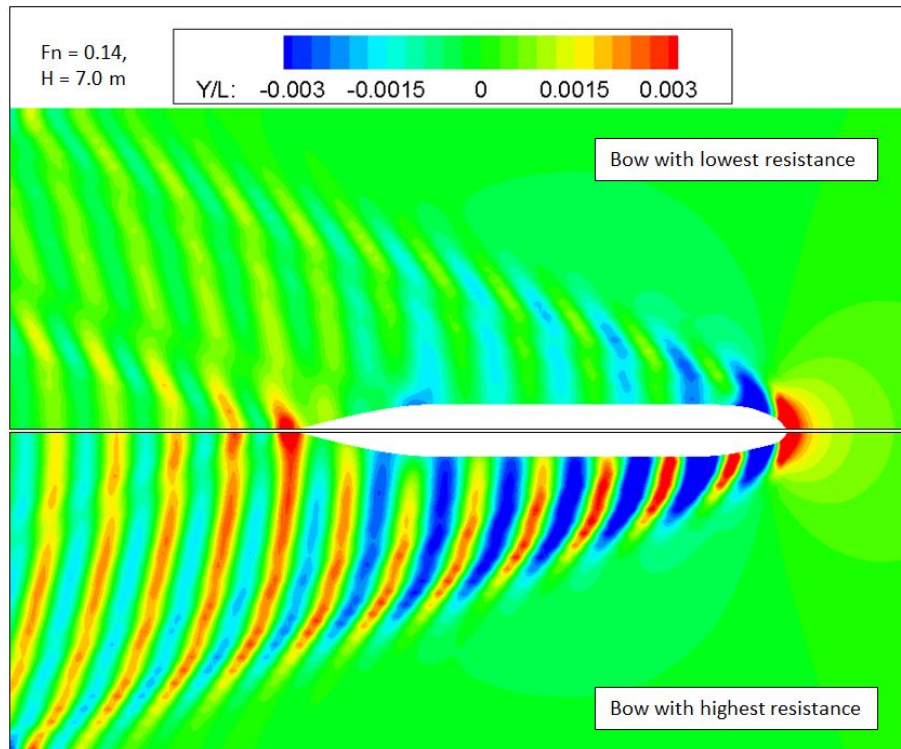


**Figure 5-9:** Normalised wave heights for bow shapes with the highest and lowest  $Rw3$  values for  $Fn = 0.14$  and  $h = 7.0$  m



**Figure 5-10:** Waterlines plans of bow 125 (left, good resistance characteristics) and bow 65 (right, poor resistance characteristics)

a smooth transition between the bow and the parallel midship. The forward shoulder for these ships is not sharp, which is favourable for the wave making resistance. The large slope at 75% of the bow length in combination with the relative small waterline entrance angles indicates a strong increase in volume in the front part of the bow. Intuitively one would say that this leads to a high resistance, which is also explained in Section 3-2. However, it is also mentioned in that chapter that the shape of the sectional area curve at the bow is a matter of making trade-offs. If the slope of the sectional area curve in the front part of the bow would be smaller, the increase in volume has to be obtained in another part of the bow, for instance at the shoulder. That would also lead to an increase in resistance. Apparently the increase in volume can best be obtained in the front part of the bow. This is supported by the wave profiles presented in Figure 5-9. The top wave profile represents the wave pattern of bow shape 125 for  $Fn = 0.14$  and  $h = 7.0$  m (see Table 5-8), which is the best bow for this Froude number and water depth. It has a high sectional area curve slope in the front part of the bow

and a smaller slope more backwards. This bow shape generates some divergent bow waves that move away from the ship. The transverse wave system is not strong. The bottom wave profile represents bow shape 65, which is the poorest bow shape for that situation. This bow shape has a steep sectional area curve at the aft part of the bow and a more small slope of the sectional area curve in the front part of the bow. This bow shape results in a strong transverse wave system which has a negative influence on the resistance. The waterlines plans of both bows are presented in Figure 5-10. The differences between the two bow shapes can clearly be observed. The waterlines plan of bow 65 shows some bumps, leading to the unfavourable values of the sectional area curve slope. The waterlines plan of bow 125 clearly looks better.

Apart from the slope of the sectional area curve, the bow length and ship volume are also present in the linear models. However, their values are not remarkably high or low for the collection of good bows. The same holds for the parameters that are not present in the linear models. A similar analysis can be done for the poorest bows per situation. An overview of the two poorest bows per situation is presented in Table 5-9. The waterline entrance angle seems to be a dominant parameter here. All bows from the list have a high value for the waterline entrance angle, except for the second bow from the situation where  $Fn = 0.16$  and  $h = 5.5$  m. This bow has the lowest volume of the entire dataset, resulting in a high  $Rw3/\nabla$  fraction.

## 5-2 Viscous flow calculations

As described in Section 4-4, several experiments have been carried out to investigate to which extent the viscous resistance changes when the bow shape is changed. Calculations have been carried out for four bow shapes for the situation where  $Fn = 0.14$  and  $h = 5.5$  m. The results are presented in Table 5-10. It can be observed that the total resistance barely changes for the different bow shapes. The total resistance of bow shape 90 is slightly lower. This is because the wetted area is somewhat smaller. The table also gives separate friction coefficients for the dynamic pressure resistance and the frictional resistance. The frictional resistance turns out to have the largest contribution to the total resistance (about 85%).

Though the resistance values are similar for the four bow shapes, the pressure distributions may be different. The pressure distribution for the four bows is presented in Figure 5-11. It can be observed that there are indeed differences. For bow shape 26 the areas of low and high pressure coefficients are the most distinct. Bow shape 90 has the smallest areas with high and low pressures. Though the areas where high or low pressures occur are different in size,

**Table 5-10:** Results of viscous flow calculations

Bow	$Rw3$ [kN]	$A_{wet}$ [m <sup>2</sup> ]	$Cd_{p_{dyn}}$	$Cd_f$	$Cd_{tot}$	$R_{tot}$ [kN]
11	11.22	1660	3.199E-04	1.933E-03	2.250E-03	39.49
14	7.65	1667	3.273E-04	1.934E-03	2.258E-03	39.81
26	5.71	1670	3.253E-04	1.943E-03	2.256E-03	39.84
90	8.46	1656	3.039E-04	1.926E-03	2.229E-03	39.03

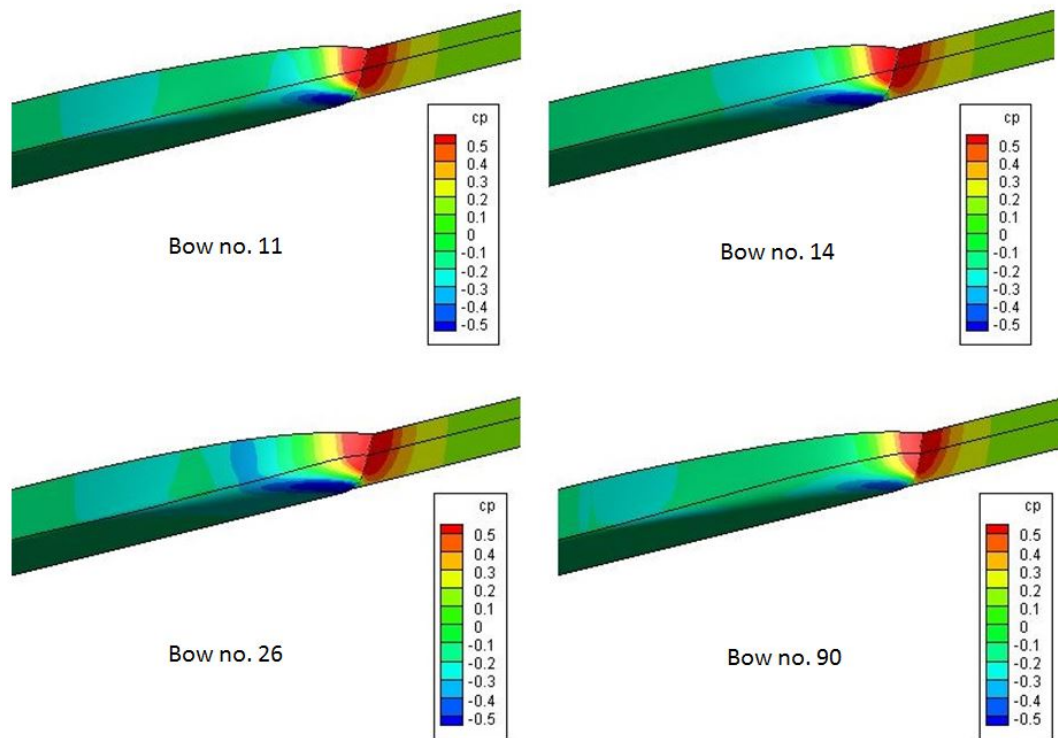


**Figure 5-11:** Pressure coefficients for viscous flow calculations

the resulting net force remains similar. These forces are so similar that the differences in the wave making resistance are much more dominant. Hereby the original assumption that the bow shape influences the wave making resistance the most, is confirmed.



---

## Chapter 6

---

### Discussion

Before conclusions are drawn from the results obtained in Chapter 5, a closer look is taken at the quality of the research and the potential uncertainties that may have occurred. This makes it possible to place the conclusions in the right perspective. Section 6-1 focusses on the quality of the method that is used for the generation of the bow geometries. In Section 6-2 several remarks on the wave making resistance are presented. Section 6-3 focusses on the quality of the fitted linear models.

#### 6-1 Bow geometry generation

A considerable part of this research consisted of defining the different bow geometries. As described in Section 4-2, this is done with a loose loft function based on six curves that describe the bow shape. For four of these curves the points can be varied, resulting in the different shapes. As described in that section, this also can result in bows with unrealistic shapes. These are filtered out, but with the current bow shape defining method, it is still possible that the remaining bows contain a kind of "lumps" that are not present in realistic bow shapes. This can happen for instance when two subsequent curves are very similar to each other, while the third subsequent curve has a very different shape. This problem could be solved by defining the bow shape with fewer curves. However, this also leads to fewer point locations that can be varied, resulting in less variability in the bow shapes.

Another point of attention of the bow shapes is the relation between the generated bow shapes and bow shapes as they are in practice. Attention is paid to obtain a realistic radius between the bottom and the side of the bow. Initially this radius was too small, leading to sharp transitions that are not often applied in practice because they lead to a high viscous resistance. This has been altered to obtain more realistic round curves. However, no further research is carried out to gain more insight the bow shapes of real inland ships, since lines plans of inland ships are in general not public and the available time was limited. It is therefore not clear to which extent the bow shapes of these research are representative for

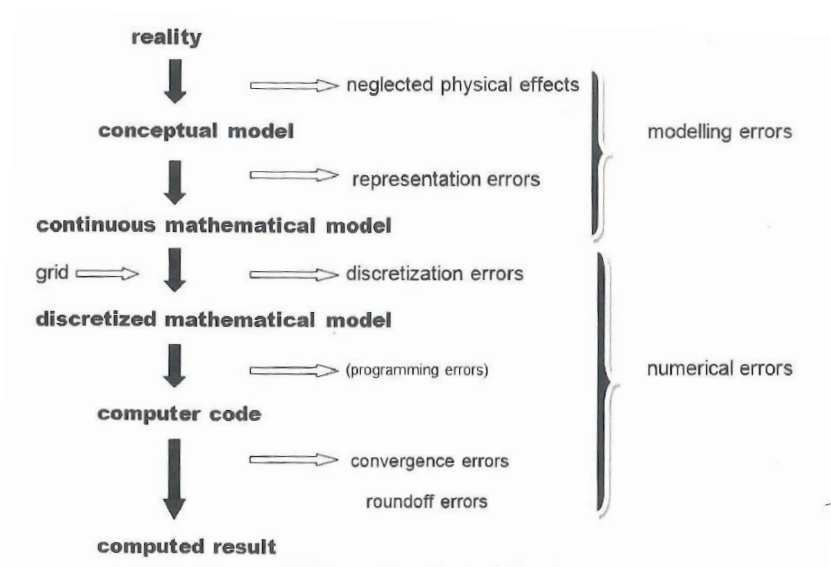


**Figure 6-1:** Sources of errors in numerical resistance calculations, retrieved from (Larsson and Raven, 2010)

real inland ships. For example, the range of the waterline entrance angles is 57.8 - 86.3 degrees (see Table 4-5 in Section 4-3). In practice bows with smaller waterline entrance angles exist (Goris, B., personal communication, 27 May 2016). Such bow shapes are not covered in this research.

## 6-2 Wave making resistance

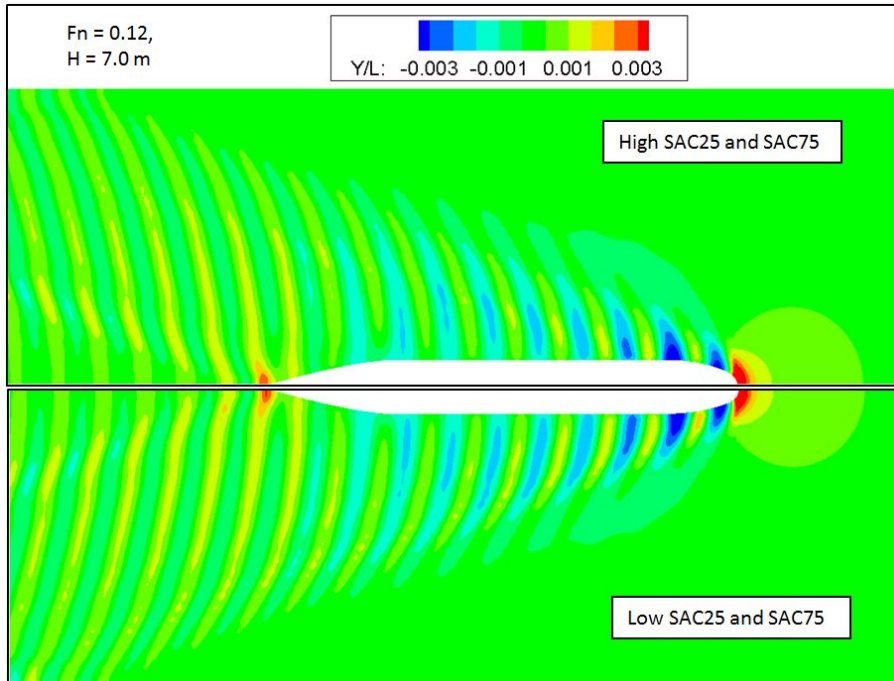
Numerical resistance calculations are subjected to several sources of error. This also applies to the obtained  $R_{w3}$  values. To gain more insight in these errors, an overview of all sources of errors is presented in Figure 6-1. The first error occurs in the transition of the reality to the conceptual model, where physical effects are neglected. In RAPID viscosity is neglected. This leads to an overestimation of the stern wave profile, which introduces the first error. In the next step the conceptual model is transferred to a continuous mathematical model. This introduces representation errors, such as linearisations. Another example of this is that the waves behind the stern are regarded as deep water waves. However, the experiments are carried out for a limited water depth. This leads to a deviation of the wave spectrum and the wave making resistance (Raven, H., personal e-mail communication, 26 April 2016). Subsequently, the continuous mathematical model is discretised. The continuous hull shape is converted to panels. Furthermore, numerical methods are used to approximate the actual values. During this process, derivatives and integrals are converted to differences and sums, in which higher order terms are neglected. The discretised mathematical model is converted to computer code and this computer code provides the final result. This final result is subjected to convergence errors and round-off errors. The convergence criterion in general states that the changes in wave heights are less than  $10^{-4}$  times the ship length in the entire domain. More information about the numerical accuracy of RAPID can be found in (Raven, 1996).

The low Froude numbers are a phenomenon that cause additional numerical difficulties. For these cases, the hydrodynamic pressure, which has to be integrated to obtain the wave making resistance, has a very small magnitude compared to the hydrostatic pressure. This can be overcome by subtracting the hydrostatic pressure. Due to d'Alembert's paradox the hydrostatic pressure should be theoretically zero, but in practice this can not be obtained due to numerical uncertainties. When the hydrodynamic pressure is small compared to the hydrostatic pressure, these numerical uncertainties become substantial. Furthermore the most forward strips are usually subjected to pressures that are very large compared to the wave making resistance of the entire ship. Small changes in the geometry of these forward panels could have drastic consequences for the computation of the wave making resistance. Pressure integration, which results in the  $Rw1$  value, should therefore be carried out with large caution for low Froude numbers. Also the computation of the  $Rw3$  value encounters difficulties for low Froude numbers. The wave heights in such situations are small. The convergence error therefore becomes relatively large. This could be a cause for the large scatter in the  $Rw3$  values that is found for the lowest Froude number (see for instance Figure B-5 in Appendix B). The calculations could therefore better have been carried out with a stricter convergence criterion.

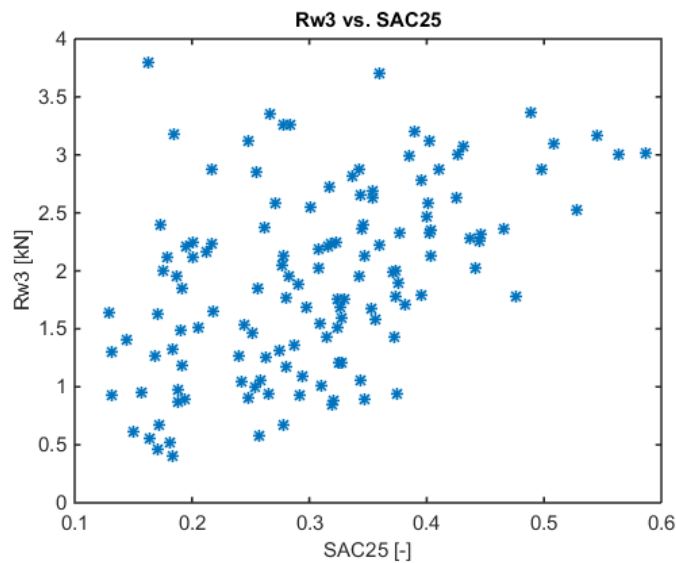
## 6-3 Linear models

Though the linear models give interesting insights in the influence of the bow shape parameters on the wave making resistance, the results should be taken with caution. As mentioned in Section 5-1-2, the coefficients for the bow length and the slope of the sectional area curve show some unexpected behaviour. It was expected that longer bows lead to a lower wave making resistance, but according to the linear models, this only applies for the lowest Froude number. For certain combinations of bow lengths and Froude numbers, it could happen that the bow wave interferes in an unwanted way with the wave of the shoulder, i.e. that the waves amplify each other. If that happens, even a longer bow could result in a higher wave making resistance. Furthermore the signs of  $SAC25$  and  $SAC75$  are both negative for the models where  $Fn = 0.12$ . This would imply that both values could best be as high as possible. However, in Paragraph 5-1-3 it was concluded that  $SAC25$  could better be as low as possible. To investigate why the signs of both parameters are negative for  $Fn = 0.12$ , two wave patterns are plotted: one with high values for both parameters and one with low values for both parameters (Figure 6-2). According to the linear model, the one with the high values for both parameters should lead to lower resistance. However, in Figure 6-2 a difference can barely be observed. Therefore there must be another reason that the sign of  $SAC25$  is negative. To gain more insight in this, the relation between  $SAC25$  and  $Rw3$  is plotted in Figure 6-3. The result is remarkable. Though a higher  $SAC25$  leads to a lower wave making resistance according to the linear model, the figure shows that a higher  $SAC25$  leads to a higher  $Rw3$  value, which is in line with the expectations. However, there are several outliers with a low  $SAC25$  and a high  $Rw3$  value (top left in the figure). These points deviate strongly from the trend and could be the cause of the negative sign of  $SAC25$  in the linear model.

Another point of attention can be observed in the statistical plots presented in Appendix B. It can be observed in the plots of the difference between the fitted models and the  $Rw3$  values



**Figure 6-2:** Normalised wave heights for bow shapes with high and low values for  $SAC25$  and  $SAC75$ , for the situation where  $F_n = 0.12$  and  $h = 7.0$  m

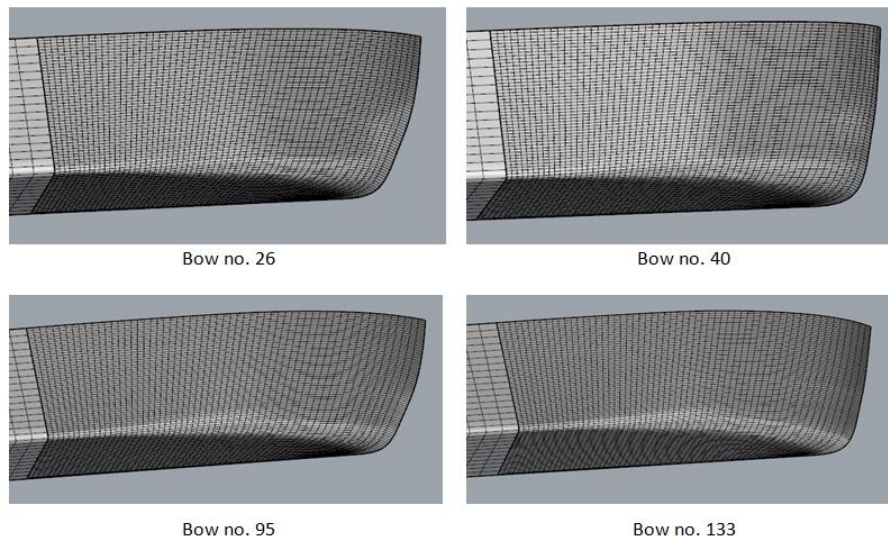
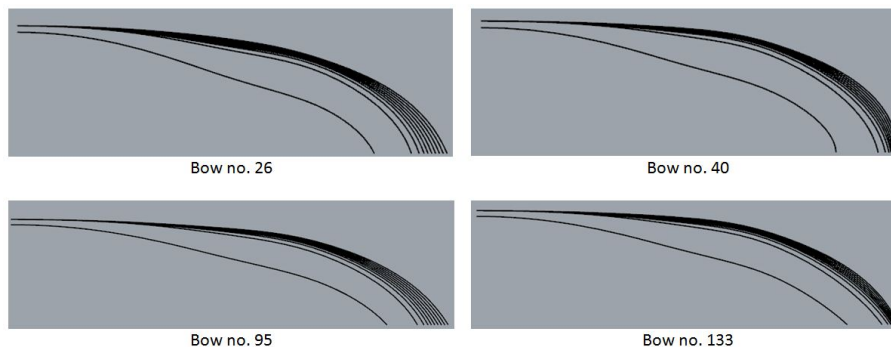


**Figure 6-3:**  $Rw3$  vs.  $SAC25$  for  $F_n = 0.12$  and  $h = 7.0$  m

that the wave making resistance of some individual bow shapes can not be predicted well by the model. An overview of these bow shapes leading to large inaccuracies is given in Table 6-1. The values for the parameters are normalised with the difference between the maximum and the minimum parameter values of the total data set in order to get a quick insight in how extreme the parameter values are. Bow shapes 26, 95 and 133 have large deviations for mul-

**Table 6-1:** Normalised parameters for bow shapes with inaccurate resistance prediction

Bow no.	Lbow	Vship	$\alpha$	$\beta$	Cwp	SAC25	SAC75	T25
26	0.34	0.65	0.36	0.21	0.47	0.40	1.00	0.74
40	0.17	1.00	0.80	0.99	0.85	0.13	0.95	0.90
95	0.97	0.48	0.03	0.14	0.60	0.12	0.79	0.87
133	0.75	0.68	0.04	1.00	0.63	0.09	0.85	0.91

**Figure 6-4:** Geometries of bows leading to inaccuracies with resistance prediction**Figure 6-5:** Waterlines plans of bows presented in Figure 6-4

tiple combinations of Froude numbers and water depths. Bow number 40 has large deviations only for the situation where  $Fn = 0.14$  and  $h = 5.5$ . It is remarkable that all these bow shapes contain one or more extreme values for the parameters. A graphical view of these bows is given in Figure 6-4 (note that the bows are enlarged in the vertical direction for computation purposes, see Paragraph 4-3-2). The waterlines plans of these bow shapes are presented in Figure 6-5. It can be observed that bow number 40 has indeed a very large volume, as is indicated in Table 6-1. The inaccuracies for these bows in the linear model are likely to have a computational origin. This can be supported by having a closer look in the way the linear

models are obtained. For two situations ( $Fn = 0.12, h = 5.5$  and  $Fn = 0.16, h = 5.5$ ) the first normal probability plot shows some outliers. To obtain a better model, these outliers are excluded from the model. This implies that the wave making resistance of the outliers itself can not be estimated adequately any more. Bow shapes 26 and 133 turn out to be two of those outliers. RAPID might encounter difficulties in computing the  $Rw3$  value due to the extreme values for several bow shape parameters.

# Conclusions

The goal of this research was to generate a guideline that can be used to assess the influence of the bow shape of inland ships on the resistance. The associated main research question was:

*What is the influence of bow shape parameters on the resistance of an inland ship?*

Numerical resistance experiments for a set of different bow shapes have been carried out to answer the research question. First it has been investigated which parameters were to be included in the research. Ten parameters were defined, from which eight of them describe the shape of the bow and two describe sailing in restricted water. For various combinations of the parameters, the wave making resistance has been calculated with the panel code RAPID. The  $Rw_3$  values that are returned by RAPID is used as a measure for the wave making resistance. These values are suitable for comparing different bow shapes, but not suitable for predicting the absolute value of the resistance. Statistical analysis was carried out on the results to determine which bow shape parameters influence  $Rw_3$  the most. It turns out that the **slope of the sectional area curve**, the **bow length** and the **ship volume** have the largest effect on the wave making resistance. This holds for all Froude numbers and water depths that are considered. The influence of these four parameters on the wave making resistance can be quantified with linear models. This answers the main research question. However, the results are still subjected to several major restrictions:

1. The  $Rw_3$  values from RAPID contain a relative high level of uncertainty, since the calculations are carried out for low Froude numbers.
2. The linear models **can not** be used for predicting the absolute value of the wave making resistance, since they are based on  $Rw_3$  values. These values are suited more for comparing different shapes than for predicting the absolute value of the wave making resistance.

3. The coefficients for the different terms in the linear models are strongly dependent on outliers in the obtained resistance data. For some cases this leads to results that are not in line with what was expected based on physical phenomena.

In practice the bow design of an inland ship is a trade-off between the resistance and the load capacity. The results of the research show that bows with a smooth shoulder and a high increase of volume at the front part of the bow lead to a relative low resistance compared to the ship volume. This bow type generates mostly divergent waves, which do not contribute to the wave making resistance as much as transverse waves.

It was originally assumed that the viscous resistance does not change significantly when the bow shape is changed. This assumption is supported by viscous double body flow calculations for several bows at a representative Froude number and water depth.

# Recommendations

Although the main research question is answered, some aspects can be improved or researched more thoroughly.

An important restriction of the presented method is that it is only able to compare different bow shapes and does not give an accurate estimate for the absolute value of the wave making resistance. Therefore it is difficult to draw conclusions about how large the effect of changing the bow shape is on the total ship resistance. This should be investigated more thoroughly before further research is initiated. Based on the result of this analysis it can be decided whether it is useful to carry out further research on the bow shape of inland ships.

If further research turns out to be useful, it is recommended to investigate first whether numerical resistance prediction methods can be improved for low Froude numbers, since low sailing speeds are characteristic for inland ships. Another option could be to carry out empirical experiments in a towing tank. Since this does not require discretisation of the mathematical model, numerical uncertainties can be significantly reduced. If both numerical and empirical data would be available, more grounded conclusions about the influence of the bow shape on the resistance could be drawn.

With more reliable values for the resistance, more reliable statistical models can be generated. When such models for the bow shape and the stern shape are combined, an adequate and detailed resistance prediction method for inland ships can be developed. This could be an improvement, since most current resistance prediction methods are outdated, do not contain a significant level of detail or do not apply especially to inland ships.

Finally, this research can be placed in a more broad context. The eventual purpose of investigating the influence of the bow shape on the resistance is to search for measures that can reduce the fuel consumption of inland ships. The hull design is only one factor that is related to that purpose. Other improvements can be obtained by e.g. increasing the engine efficiency or adapting the navigational behaviour of the captain. An intensive collaboration between

ship designers, ship owners and research institutes is needed to study fuel consumption in the full context of the problem.

---

# Bibliography

- Bureau Voorlichting Binnenvaart (2013). Waardevol Transport - De toekomst van het goederenvervoer en de binnenvaart in Europa 2013-2014. Bureau Voorlichting Binnenvaart, Rotterdam.
- de Koning Gans, H. (2012). Introduction of Numerical Methods in Ship Hydromechanics. Delft.
- European Environment Agency (2013). The impact of international shipping on European air quality and climate forcing. Copenhagen.
- Heuser, H. (1986). Verdrängungsschiffe auf flachem Wasser. *Schiffstechnik*, Volume 33, no. 1, pages 22–26.
- Heuser, H. (1987). Neue Entwicklungen beim Entwurf von Flachwasserschiffen. *Duisburger Kolloquium Schiffstechnik/Meerestechnik*, Volume 8.
- Kim, H., Jeong, S., Yang, C., and Noblesse, F. (2011). Hull Form Design Exploration Based on Response Surface Method. In *Twenty-first International Offshore and Polar Engineering Conference*, Maui.
- Klein Woud, H. and Stapersma, D. (2012). *Design of Propulsion and Electric Power Generation Systems*. IMarEST, London.
- Lane, D. (2016). Online Statistics Education: A Multimedia Course of Study. <http://onlinestatbook.com/>, accessed May 2016
- Larsson, L. and Raven, H. (2010). *Ship Resistance and Flow*. The Society of Naval Architects and Marine Engineers, Jersey City, 1st edition.
- Ledolter, J. and Hogg, R. (2010). *Applied Statistics for Engineers and Physical Scientists*. Prentice Hall, Upper Saddle River, 3rd edition.
- MARIN (2015a). PARNASSOS.  
<http://www.marin.nl/web/Facilities-Tools/CFD/PARNASSOS.htm>, accessed October 2015

- MARIN (2015b). RAPID User's Guide, version 4.5.1.
- MARIN (2015c). REFRESCO.  
<http://www.marin.nl/web/Facilities-Tools/CFD/ReFRESCO.htm>, accessed October 2015
- MathWorks Documentation (2016). Linear regression.  
<http://nl.mathworks.com/help/stats/linear-regression-model-workflow.html#btb50q6>, accessed May 2016
- Netherlands Government (1995). Wetten Overheid.  
<http://wetten.overheid.nl/BWBR0007858/2009-01-01>, accessed December 2015
- Numeca International (2015). FINE/Marine - Key features.  
<http://www.numeca.com/en/products/finetmmarine>, accessed October 2015
- Raven, H. (1996). *A solution method for the nonlinear ship wave resistance problem*. PhD thesis, Delft University of Technology.
- Raven, H. (2012). A computational study of shallow-water effects on ship viscous resistance. In *29th Symposium on Naval Hydrodynamics*, Gothenburg.
- Raven, H. and Prins, H. (1998). Wave pattern analysis applied to nonlinear ship wave calculations. In *13th International Workshop on Water Waves and Floating Bodies*, Wageningen. MARIN.
- Rotteveel, E., Hekkenberg, R., and Liu, J. (2014). Design guidelines and empirical evaluation tools for inland ships. In *European Inland Waterway Navigation Conference*, Budapest.
- Schneekluth, H. and Bertram, V. (1998). *Ship Design for Efficiency and Economy*. Butterworth-Heinemann, Oxford, 2nd edition.
- The Minitab Blog (2016). Regression Analysis: How to Interpret the Constant (Y Intercept).  
<http://blog.minitab.com/blog/adventures-in-statistics/regression-analysis-how-to-interpret-the-constant-y-intercept>, accessed May 2016
- van Terwisga, T. (1989). Weerstand en voortstuwing van bakken; een literatuurstudie. Maritime Research Institute Netherlands, Wageningen.
- Wang, G. (2003). Adaptive Response Surface Method Using Inherited Latin Hypercube Design Points. *Journal of Mechanical Design*, 125:210–220.
- Watson, D. (1998). *Practical Ship Design*. Elsevier, Oxford, 1st edition.

# Alternative wave making resistance prediction method

As mentioned in Chapter 5, the  $Rw3$  values from the RAPID output have been used to base the analysis of the results on. Though  $Rw3$  is very useful to compare different bow shapes, it is less suitable for predicting the absolute value of the wave making resistance. Furthermore, some minor interference between the bow wave system and the stern wave system occurs. For these reasons it has been investigated whether the wave making resistance of the bow could also be obtained in a different way. Unfortunately this has not led to a usable result. However, the investigation provided a good insight in the physics of the wave making resistance. Furthermore, it may act as a basis for potential further research. Therefore the investigation is described in this appendix.

The wave making resistance can be obtained by integrating the local pressure over the wetted surface. To gain a better insight in this phenomenon, it is useful to evaluate of which components the pressure is built up. The total pressure consists of the hydrostatic pressure and the hydrodynamic pressure. Both have components related to the double body flow and the free surface flow. This leads to the following pressure components:

1. Hydrostatic
  - 1a) Pressure up to still waterline
  - 1b) Pressure between still waterline and free surface
2. Hydrodynamic
  - 2a) Pressure in double body flow
  - 2b) Pressure difference between double body flow and flow with free surface

When a closed body in a potential flow is considered, components 1a and 1b cancel due to d'Alembert's paradox. Components 1b and 2b, which are related to wave making, remain.

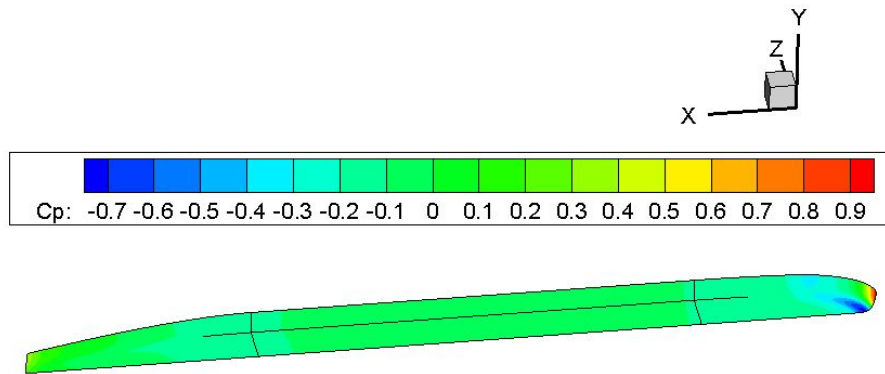


**Figure A-1:** Pressure coefficients in double body flow

The  $Rw1$  and  $Rw3$  values that are calculated by RAPID consider these two components. However, due to the neglect of viscosity, RAPID is unable to compute the wave profile at the stern in a physical realistic way. To determine the influence of the bow shape on the wave making resistance, it would therefore be adequate to isolate the bow and integrate the pressures of that segment only. However, the bow on itself is not a closed body. Therefore the pressure components 1a and 2a do not longer cancel out. Since these components are related to the flow up to the still waterline and components 2a and 2b are related only to the waves, they are expected to have a substantial larger magnitude. Therefore, they have to be calculated and subtracted from the total pressure. For component 1a this is a simple procedure. The output files of RAPID already contain the non-dimensional force coefficients per strip that are based on the total pressure minus the hydrostatic pressure up to the still waterline. The computation of the double body force from component 2a is less trivial. This is not covered in RAPID. A separate tool has been used to compute the double body force. The working principles of this method are similar to RAPID, but the difference is that no waves are generated. The output of the tool consists of the local pressure coefficients and x-, y- and z-velocities for each hull panel. From this information the double body force can be computed. Tecplot is used for this. This is a tool for visualizing and post-processing results of numerical flow calculations. First a file is generated that is compatible with Tecplot. It is not possible to load the pressure coefficients directly into Tecplot, but the compatible file contains the local velocities. From these velocities the local pressure coefficients can still be computed. These are similar to the pressure coefficients in the output file of the double body flow calculation tool. This indicates that the pressure coefficients are calculated in the right way. A contour plot of the pressure coefficients is given in Figure A-1. This figure presents the pressure coefficients for only one bow shape, but since the stern shape remains unchanged and the total force cancels out, it is sufficient to calculate the double body force for only one bow shape. The water depth still has to be included, resulting in three separate calculations. The presented pressure coefficients are for a water depth of 7.0 m. The distribution of the pressure coefficients is as expected. High pressures occur at the stagnation point at the bow. The lowest pressure coefficients occur at the bottom of the bow. The pressures are obtained by multiplying the pressure coefficients with  $\frac{1}{2}\rho V^2$ , where  $V$  is the velocity of the undisturbed flow, which is the sailing speed in this case. The calculation is evaluated for  $Fn = 0.12$ , which leads to a sailing speed of 3.94 m/s.

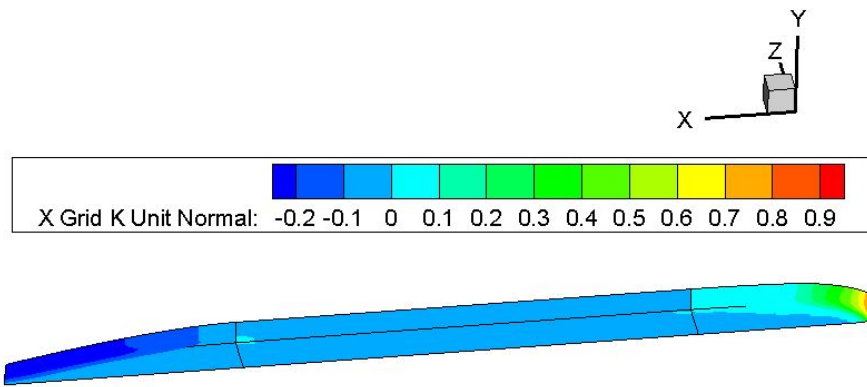


**Figure A-2:** Normal vector magnitudes in double body flow

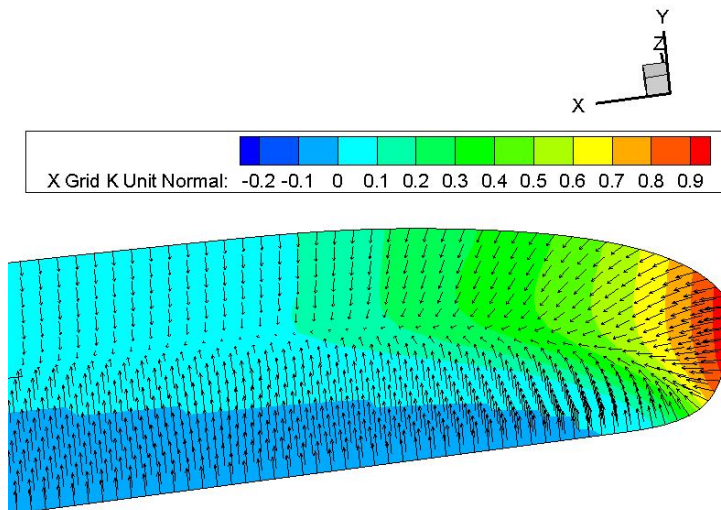


**Figure A-3:** Close-up of bow normal vectors in double body flow

Since the resistance in longitudinal direction is to be obtained, the pressure has to be multiplied with the x-component of the normals. This can be calculated with Tecplot. Figure A-2 presents the magnitude of the normal vectors. A close-up of the normal vectors of the bow is given in Figure A-3. As can be seen in this figure, the normals are pointed inward, which is compatible with the coordinate system of RAPID. The magnitude of the pressure multiplied with the x-component of the normal vector is presented in Figure A-4. This is the integrand for the integration that leads to the double body force. In the bow some locations with extreme values (both high and low) occur. The stern has a region where the values are smaller, but the region itself is larger. At the midship, the integrand is close to zero. This is in line with what could be expected, since the midship does not have a normal component in x-direction.

The integration is performed with Tecplot. The expected result is that the force on the midship is practically zero and the forces at the bow and the stern are similar, but in opposite

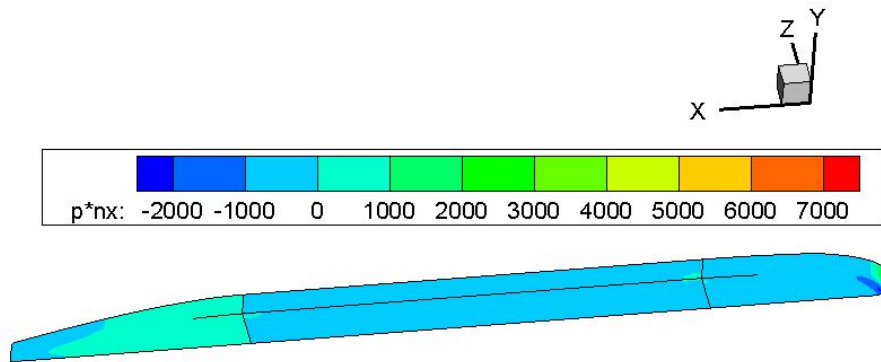


**Figure A-4:** Product of pressure and normal vectors in double body flow

**Table A-1:** Forces on different ship sections in double body flow

Ship section	Force [N]
Bow	-631
Midship	-0.14
Stern	1359
<b>Total</b>	<b>727</b>

direction. Table A-1 gives the forces on the different segments. As can be seen, the result is not as expected. The total force, which is the double body force, does not equal zero. Since the total force does not lead to the right answer, it is likely that the force components on the bow and the stern are wrong as well. When the force on the bow obtained from RAPID, which consists of components 1a, 2a and 2b, is calculated, the result is about -2300 N for this situation. The expectation is that this value contains a large negative component from the double body force (2a), for which is compensated when the double body force is subtracted. However, when this is done for the obtained value of the double body force, the wave making force on the bow equals -1670 N. This is still not the right value.

Since the double body force is not calculated in the right way, it is not possible to isolate the bow shape from the rest of the geometry. Therefore, the  $Rw3$  value from RAPID is used for the analysis of the results. It has been investigated why the double body force calculation has led to this non-physical result. The pressure distribution of the RAPID calculations has been compared with the pressure distribution of the double body flow. The major differences occur near the waterline. This is the pressure difference of interest. Other pressure differences that could lead to the incorrect double body force value were not observed. Furthermore a more dense grid has been applied for the double body force calculation. This leads to the same pressure distribution and double body force as the original calculation. Both the pressure distribution and the grid density seem to be okay. It is most likely that the error occurs in the bow or the stern, since their force values are not equal. The most forward and most aft strips are subjected to high forces. If these forces are not predicted well, it would influence the total double body force very strong. Probably this has happened here. Further investigation is however not covered in this project due to the limited available time.

## Statistical analysis plots

In Chapter 5 a statistical analysis of the results is carried out. That chapter describes the procedure and provides plots for the situation where  $F_n = 0.12$  and  $h = 7.0$  m. The statistical analysis plots of the other situations are presented in this appendix. The section titles represent the case to which the plots apply.

### B-1 $F_n = 0.12$ and $h = 4.0$ m

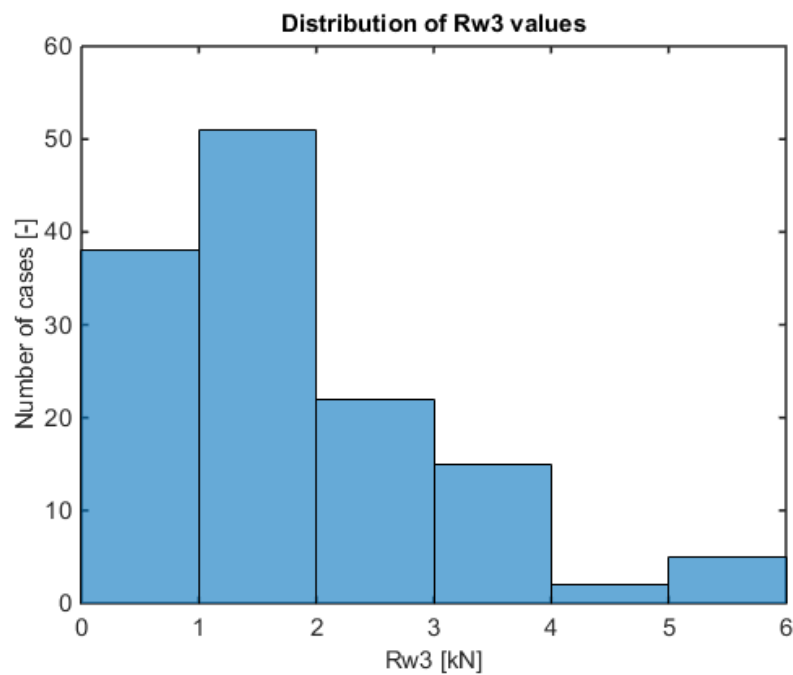
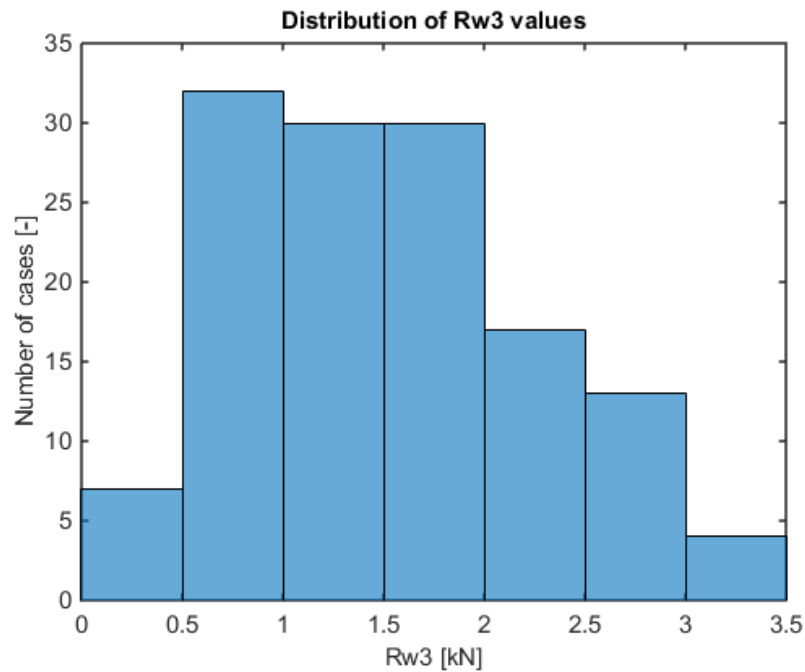
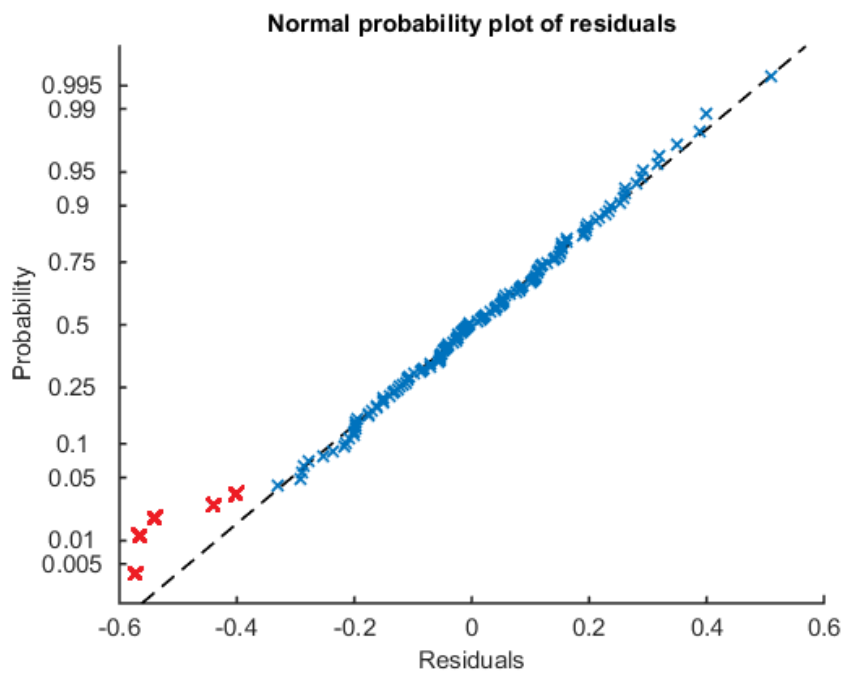
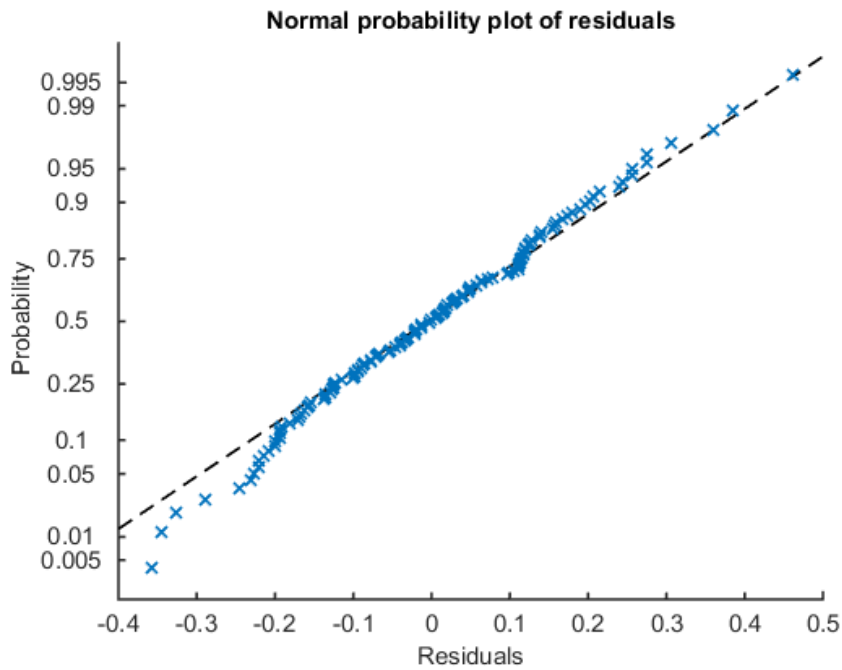
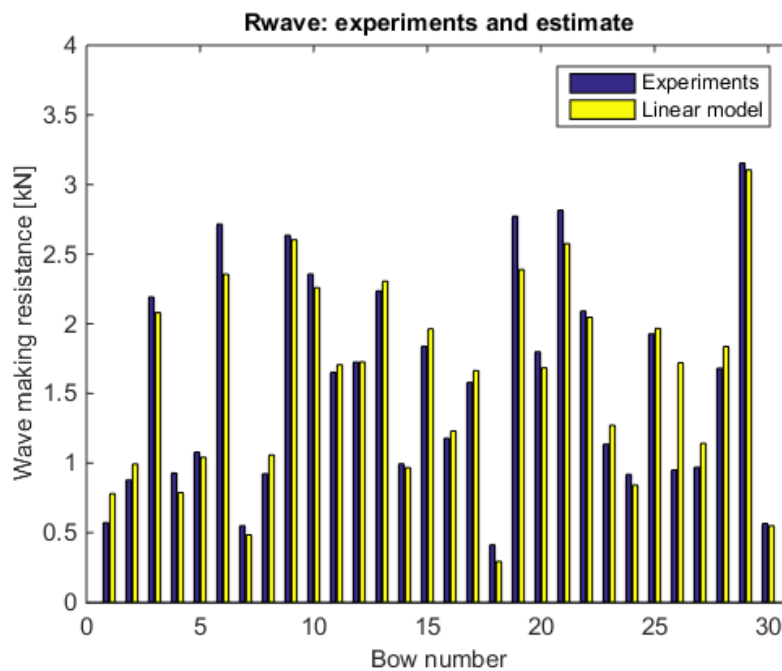


Figure B-1: Distribution of  $R_{w3}$  values

**B-2  $F_n = 0.12$  and  $h = 5.5$  m****Figure B-2:** Distribution of Rw3 values**Figure B-3:** Normal probability plot of residuals. The red crosses denote outliers.



**Figure B-4:** Normal probability plot of residuals after excluding outliers



**Figure B-5:** Comparison between  $R_{w3}$  values and values estimated with linear model

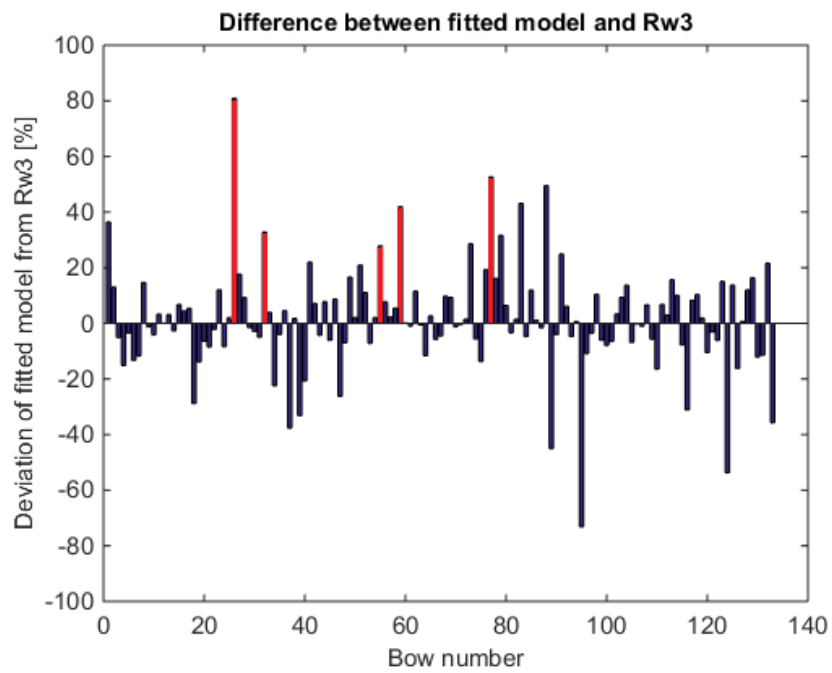


**Figure B-6:** Difference between the fitted model and the Rw3 values. The red bars denote outliers.

**B-3  $F_n = 0.14$  and  $h = 4.0$  m**

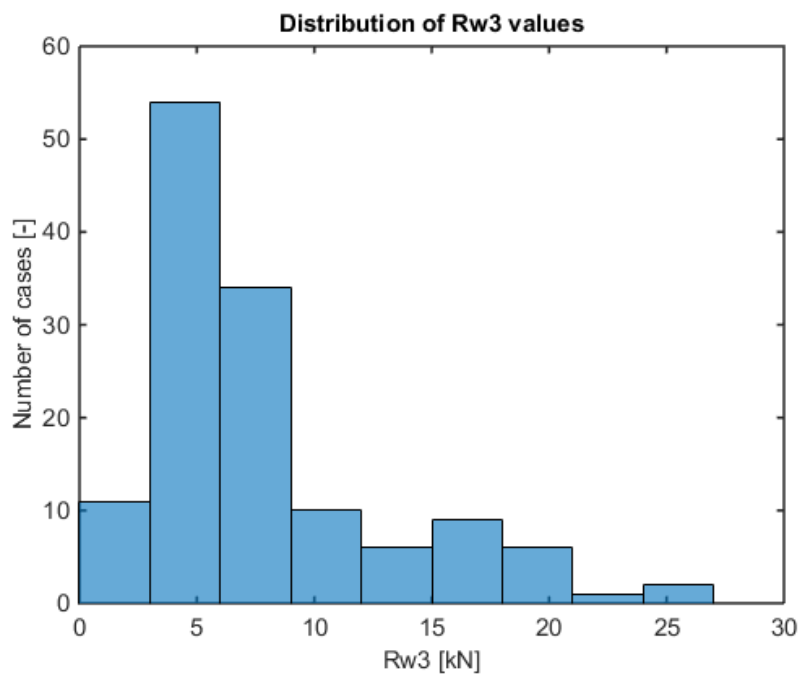


**Figure B-7:** Distribution of Rw3 values

**B-4  $F_n = 0.14$  and  $h = 5.5$  m**

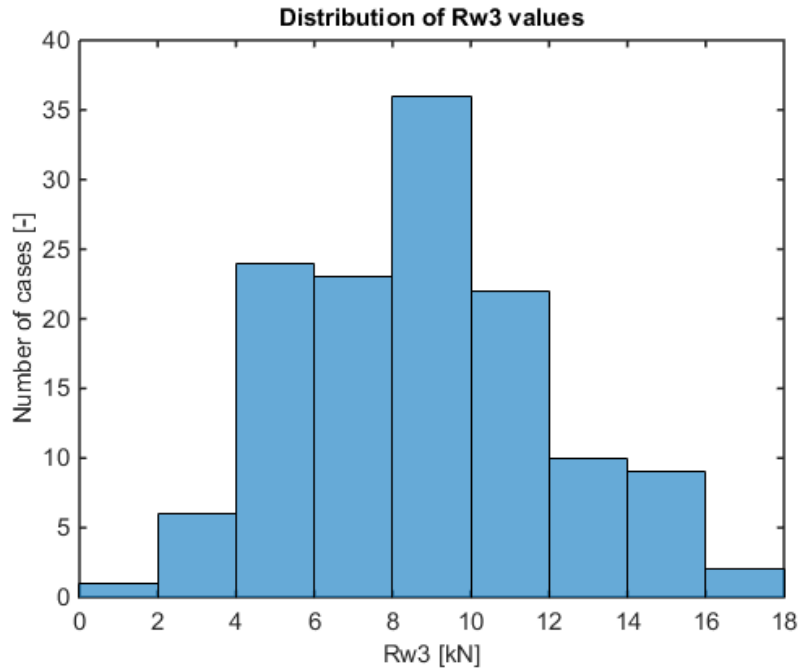


**Figure B-8:** Distribution of Rw3 values

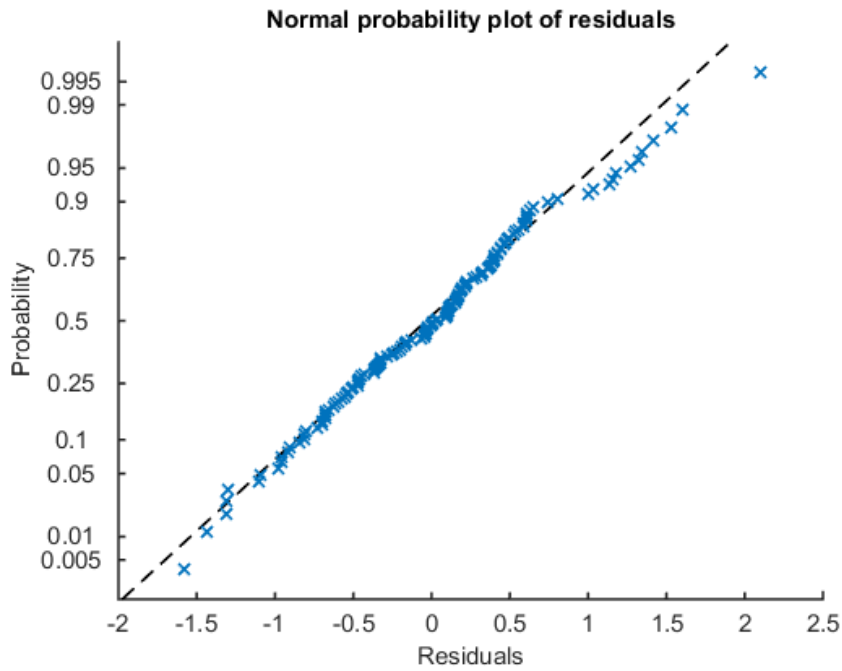


**Figure B-9:** Normal probability plot of residuals

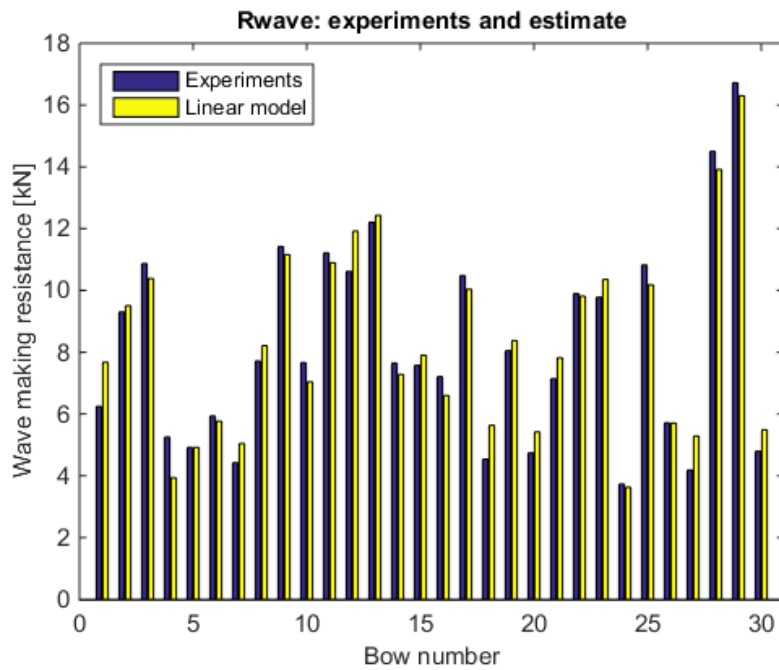


Figure B-10: Comparison between  $R_{w3}$  values and values estimated with linear model

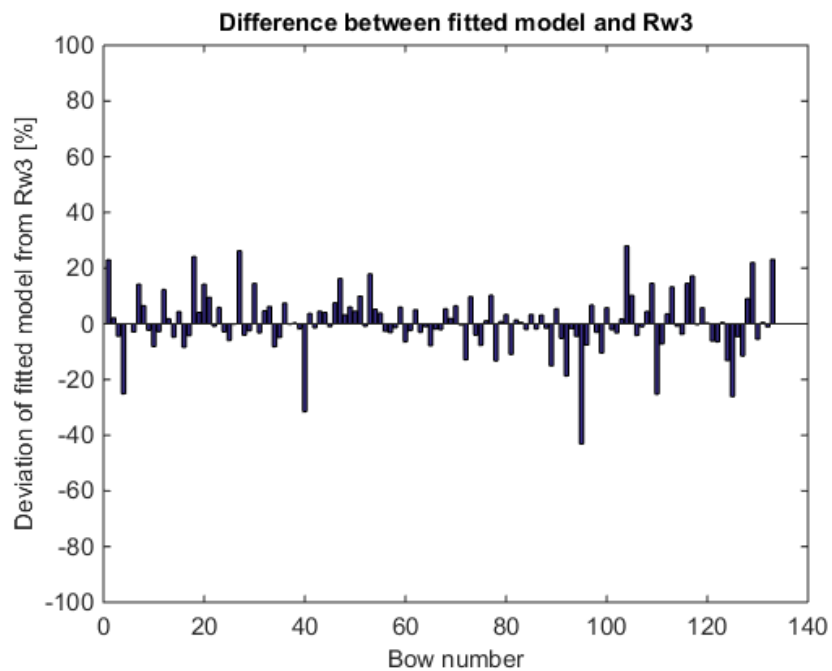
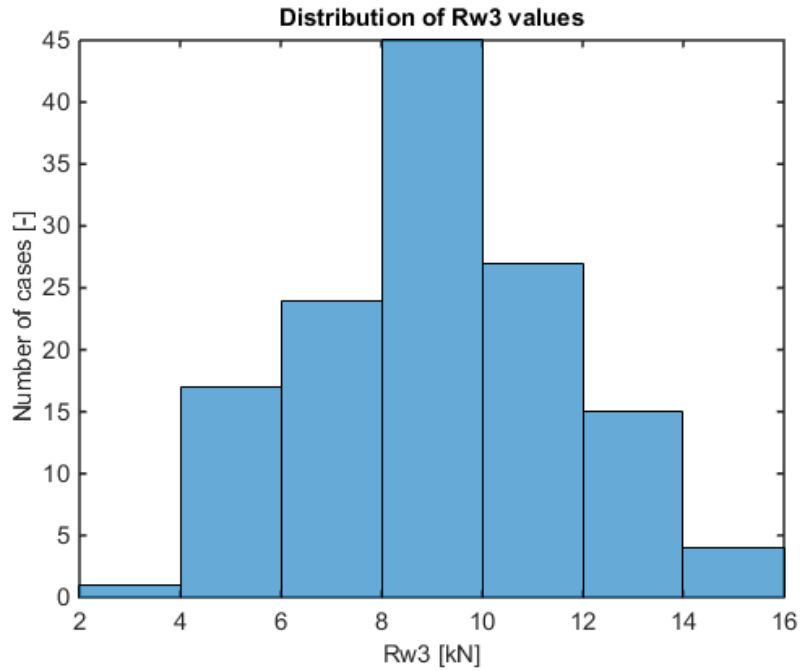
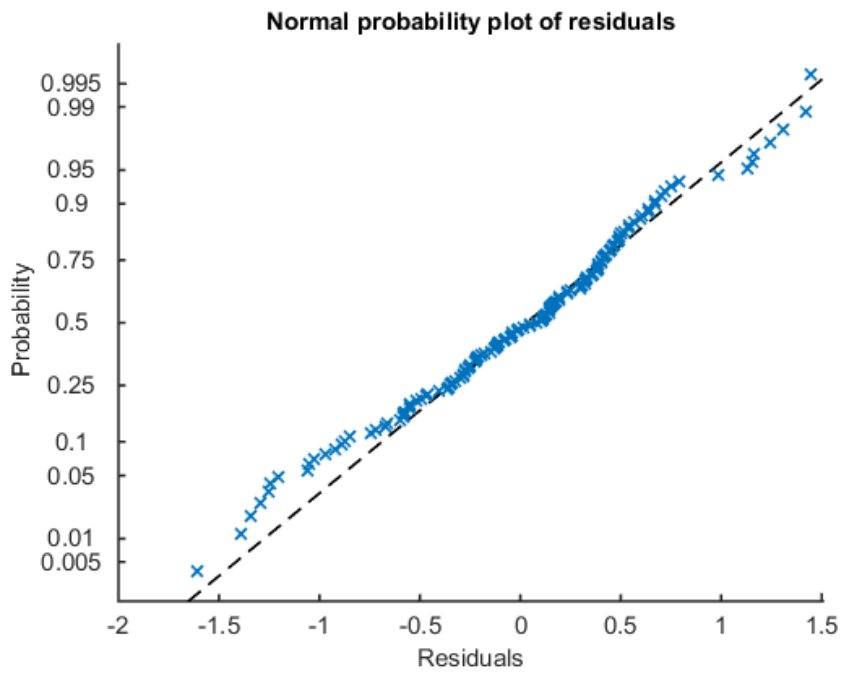


Figure B-11: Difference between the fitted model and the  $R_{w3}$  values

**B-5  $F_n = 0.14$  and  $h = 7.0$  m**



**Figure B-12:** Distribution of Rw3 values



**Figure B-13:** Normal probability plot of residuals

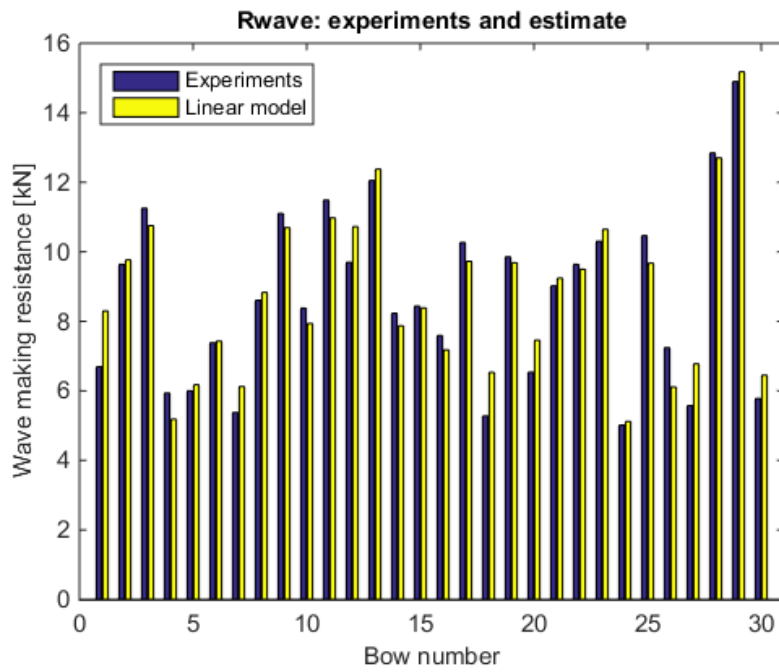


Figure B-14: Comparison between  $R_{w3}$  values and values estimated with linear model

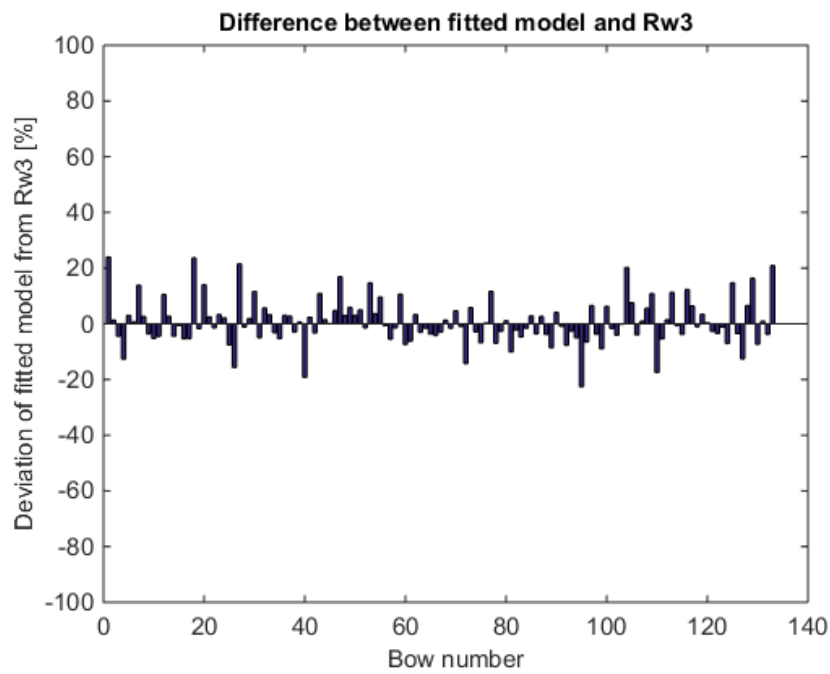
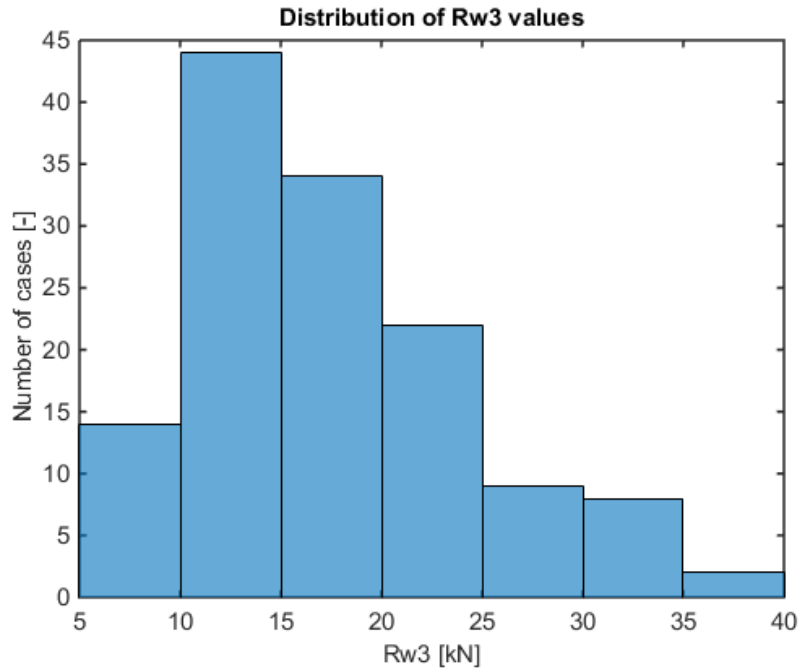
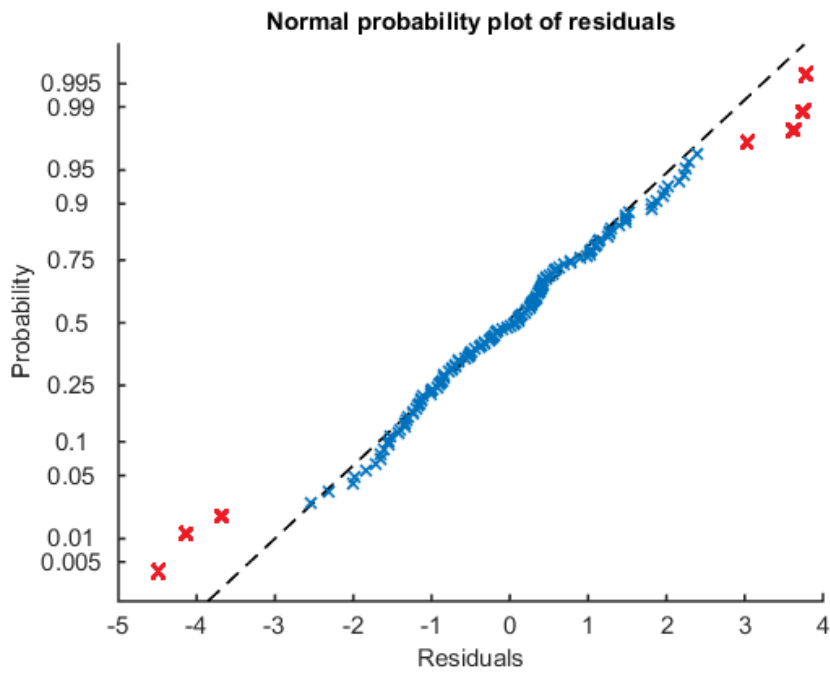


Figure B-15: Difference between the fitted model and the  $R_{w3}$  values

**B-6  $F_n = 0.16$  and  $h = 5.5$  m**



**Figure B-16:** Distribution of Rw3 values



**Figure B-17:** Normal probability plot of residuals. The red crosses denote outliers.

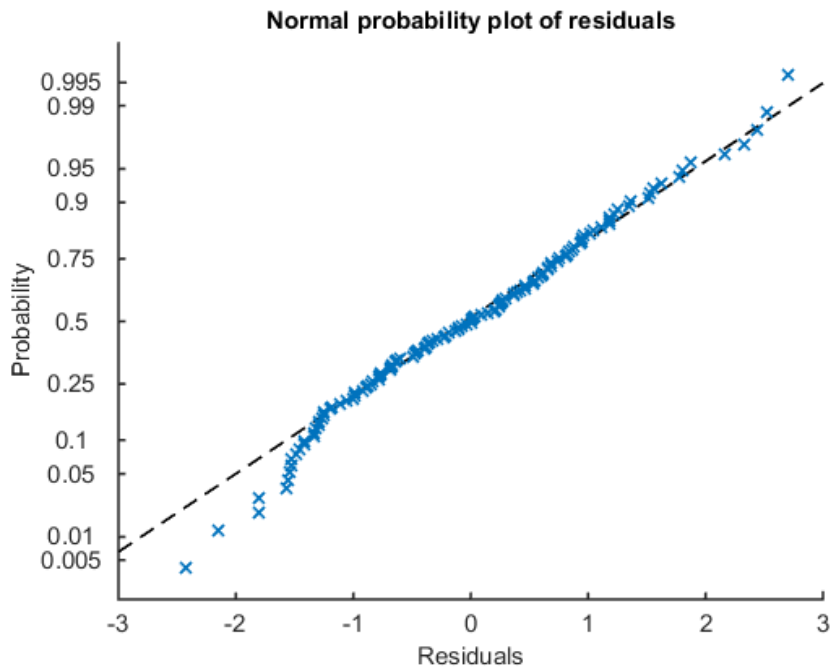


Figure B-18: Normal probability plot of residuals after excluding outliers

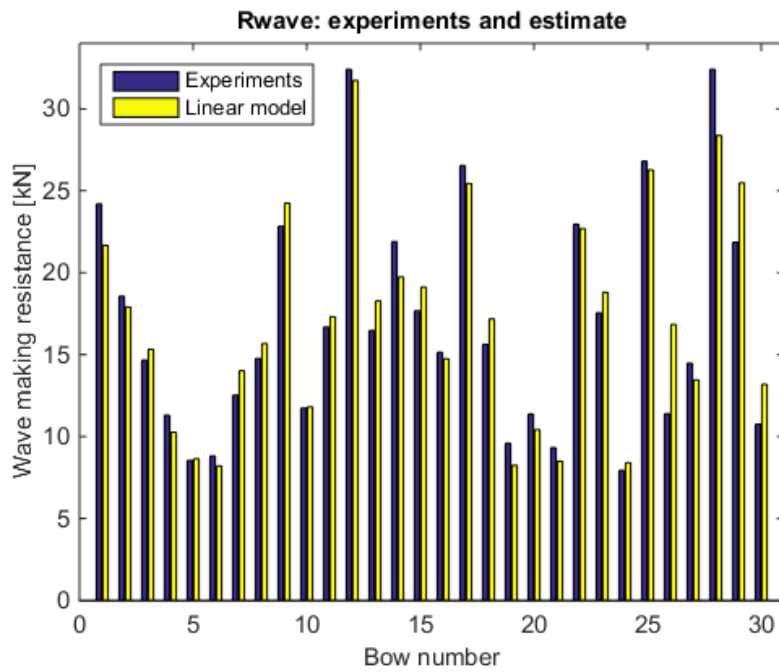
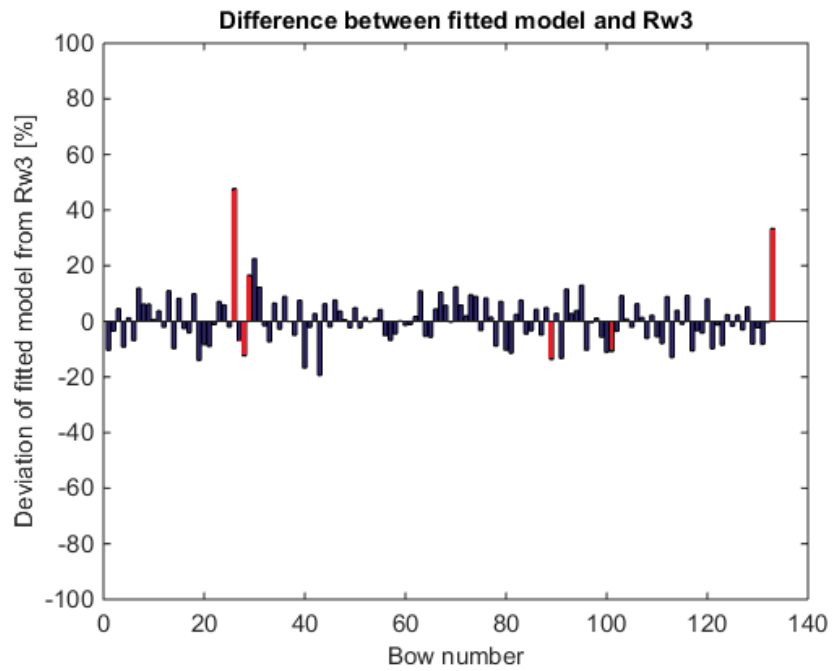
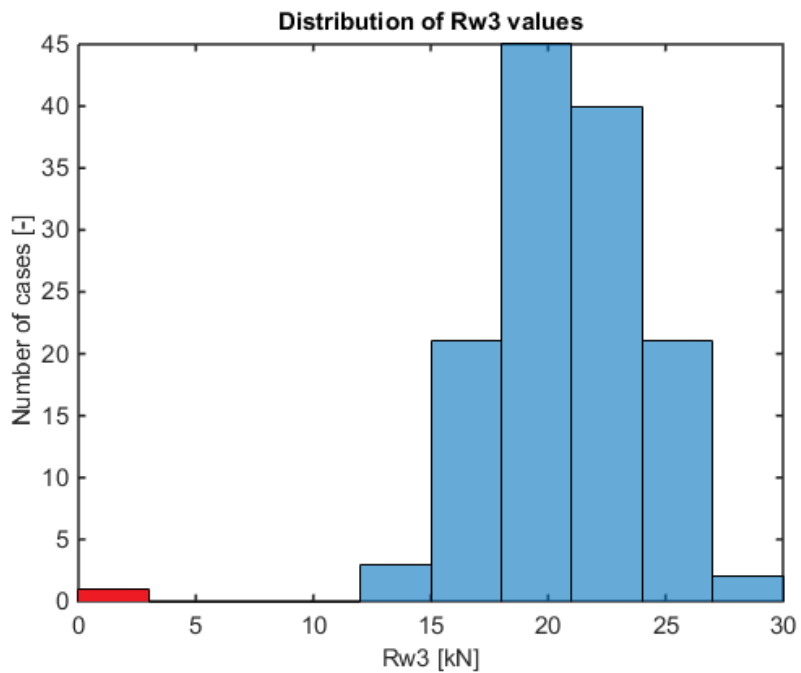


Figure B-19: Comparison between  $R_{w3}$  values and values estimated with linear model



**Figure B-20:** Difference between the fitted model and the  $R_{w3}$  values. The red bars denote outliers.

**B-7  $F_n = 0.16$  and  $h = 7.0$  m**



**Figure B-21:** Distribution of  $R_{w3}$  values. Data contains one outlier (red) due to failed calculation.

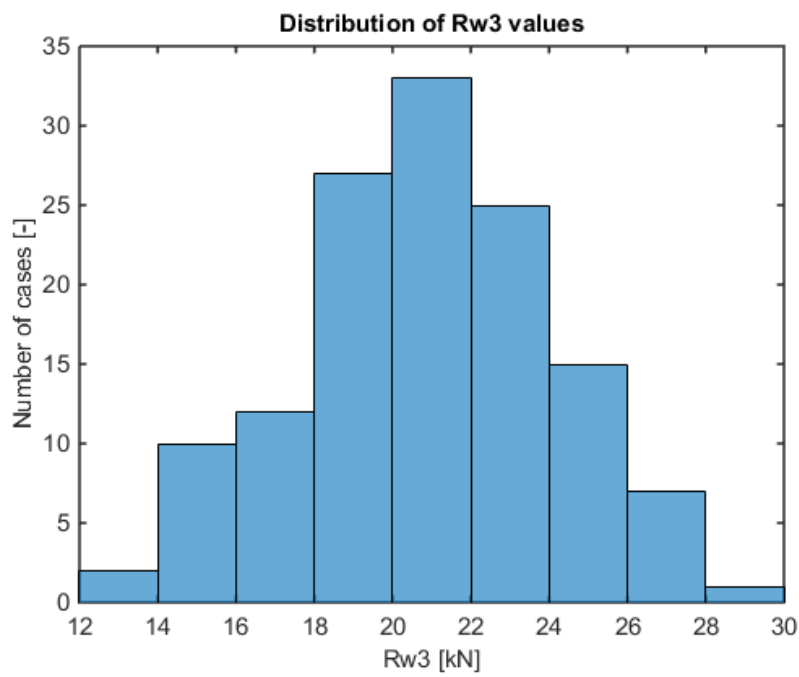


Figure B-22: Distribution of Rw3 values after removing the outlier due to the failed calculation

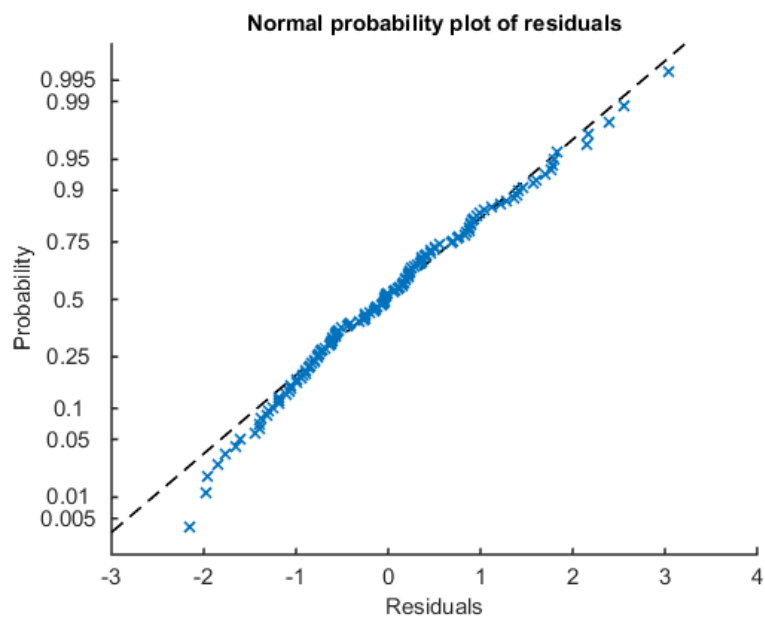


Figure B-23: Normal probability plot of residuals

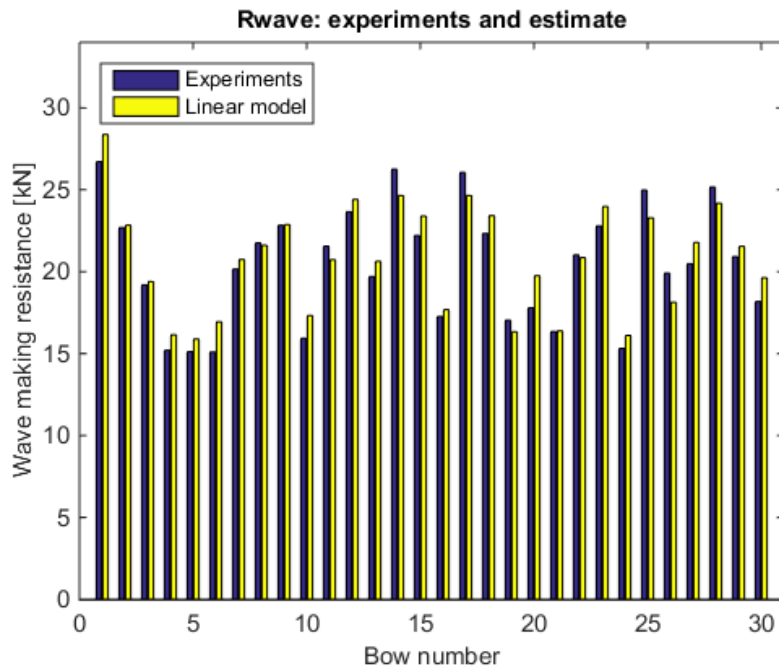


Figure B-24: Comparison between  $R_{w3}$  values and values estimated with linear model

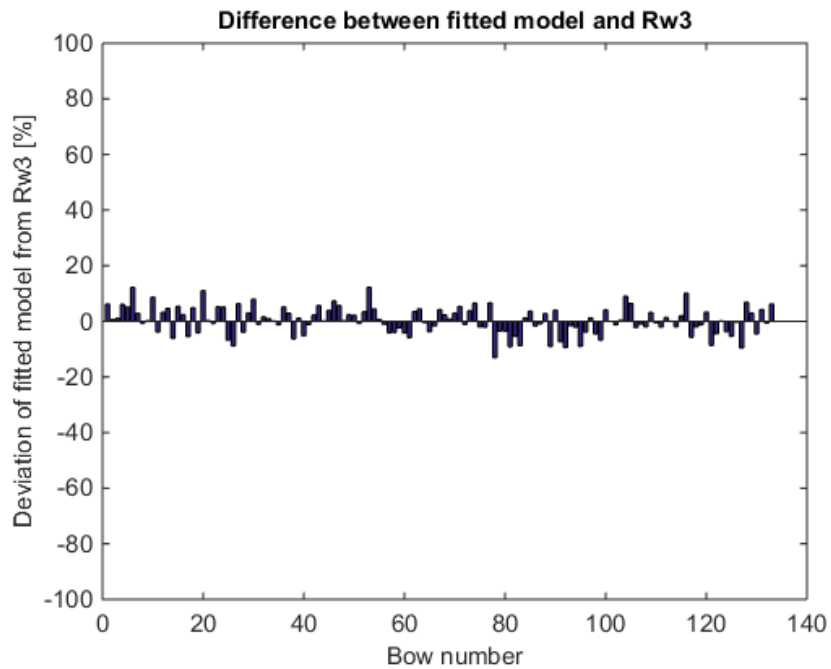


Figure B-25: Difference between the fitted model and the  $R_{w3}$  values